



Crust–mantle boundaries in the Taiwan–Luzon arc–continent collision system determined from local earthquake tomography and 1D models: Implications for the mode of subduction polarity reversal

Kamil Ustaszewski ^{a,*}, Yih-Min Wu ^b, John Suppe ^b, Hsin-Hua Huang ^b, Chien-Hsin Chang ^c, Sara Carena ^d

^a Helmholtz Centre Potsdam, GFZ German Research Centre for Geosciences, Section 3.1 Lithosphere Dynamics, Albert-Einstein-Strasse, Telegrafenberg C223, D-14473 Potsdam, Germany

^b Department of Geosciences, National Taiwan University, No. 1, Sec. 4 Roosevelt Road, 106 Taipei, Taiwan

^c Central Weather Bureau, Taipei 100, Taiwan

^d Department of Geological and Environmental Sciences, University of Munich, Germany

ARTICLE INFO

Article history:

Received 4 March 2011

Received in revised form 20 November 2011

Accepted 19 December 2011

Available online 29 December 2011

Keywords:

Taiwan

Tectonics

Earthquake tomography

Moho

Subduction

Thrust belt

ABSTRACT

In order to better understand the mode of subduction polarity reversal in the Taiwan–Luzon arc–continent collision zone, we mapped its crust–mantle boundaries using local earthquake tomography. By contouring surfaces of constant $V_p = 7.5 \text{ km s}^{-1}$, we identified three Moho discontinuities and the plate interface that juxtaposes Eurasian lower crust against mantle lithosphere of the Philippine Sea plate. The plate interface dips to the east under southeastern Taiwan and steepens progressively towards north until it becomes vertical at 23.7°N . From there it continues northward in a vertical orientation, until the limit of the tomographic model inhibited further mapping. For the Moho, additional depth constraints were derived from 1D models using P-wave arrivals of local earthquakes. The Mohos of the Eurasian and Philippine Sea plates are disconnected across the plate interface. Beneath southern Taiwan, the Eurasian Moho dips to the east at $50\text{--}60^\circ$, following the orientation of the plate boundary and continuous with the Benioff zone. Towards north, the Eurasian Moho steepens into subvertical, again together with the plate boundary. The Philippine Sea plate Moho exhibits a synform-like crustal root, interpreted as the base of the magmatic Luzon arc. Towards the north, this root deepens from 30 to 70 km underneath the Ryukyu trench. In northernmost Taiwan, the hinge of the vertically subducting Eurasian slab steps westward out of the thrust belt, leaving the deformation front to the east inactive and giving way to the north-dipping Philippine Sea plate. A subhorizontal Moho at 30–35 km depth overlies the north-dipping Philippine Sea slab and is interpreted as a newly formed Moho, established after westward rollback and delamination of the subducting Eurasian slab. In combination, these data support a model of progressive subduction polarity reversal, in which a tear within the Eurasian lithosphere propagated southwestward, deactivating the deformation front.

© 2011 Elsevier B.V. All rights reserved.

1. Introduction

The along-strike reversal of subduction polarity introduces substantial geometric complexities to the tectonics of a mountain belt at the lithosphere scale. Such polarity reversals are known from subduction-related orogens (New Zealand: e.g., McKenzie and Morgan, 1969; Taiwan: Angelier, 1986; Ernst, 1983; Suppe, 1984; Tsai et al., 1977) as well as collisional mountain belts (Pamir–Hindukush: Burtman and Molnar, 1993; Pegler and Das, 1998; Central and Eastern Alps: Kissling et al., 2006; Lippitsch et al., 2003). In Taiwan, where two subduction zones meet quasi-orthogonally (Fig. 1), contrasting models have been proposed for the mode of the subduction polarity reversal. While one model suggests instantaneous flipping across a

trench–trench transform fault between the Ryukyu and Manila trenches (Chemenda et al., 1997; Lallemand et al., 2001; Malavieille et al., 2002; Sibuet and Hsu, 2004; Suppe et al., 1981; Teng, 1990; Fig. 2a), another model invokes that subduction flip occurs by the southwestward propagation of a tear in the Eurasian lithosphere along the continental margin (Clift et al., 2003; Suppe, 1984; Fig. 2b). The second model experienced numerous variations, e.g., involving progressive breakoff of the subducting Eurasian slab during subduction flip (e.g., Molli and Malavieille, 2011; Teng et al., 2000).

In order to better understand how subduction polarity flips underneath Taiwan, we used a local earthquake tomographic model to construct 3D geometries of the various crust–mantle boundaries, i.e., (1) the plate interface separating Eurasian and Philippine Sea lithosphere, (2) the Eurasian and (3) the Philippine Sea plate Moho. Our structural model reveals, from south to north, a progressive steepening of the eastward subducting Eurasian slab into vertical. We consider this the response to the northwestward motion of the Philippine Sea

* Corresponding author. Tel.: +49 331 288 1312.

E-mail address: kamilu@gfz-potsdam.de (K. Ustaszewski).

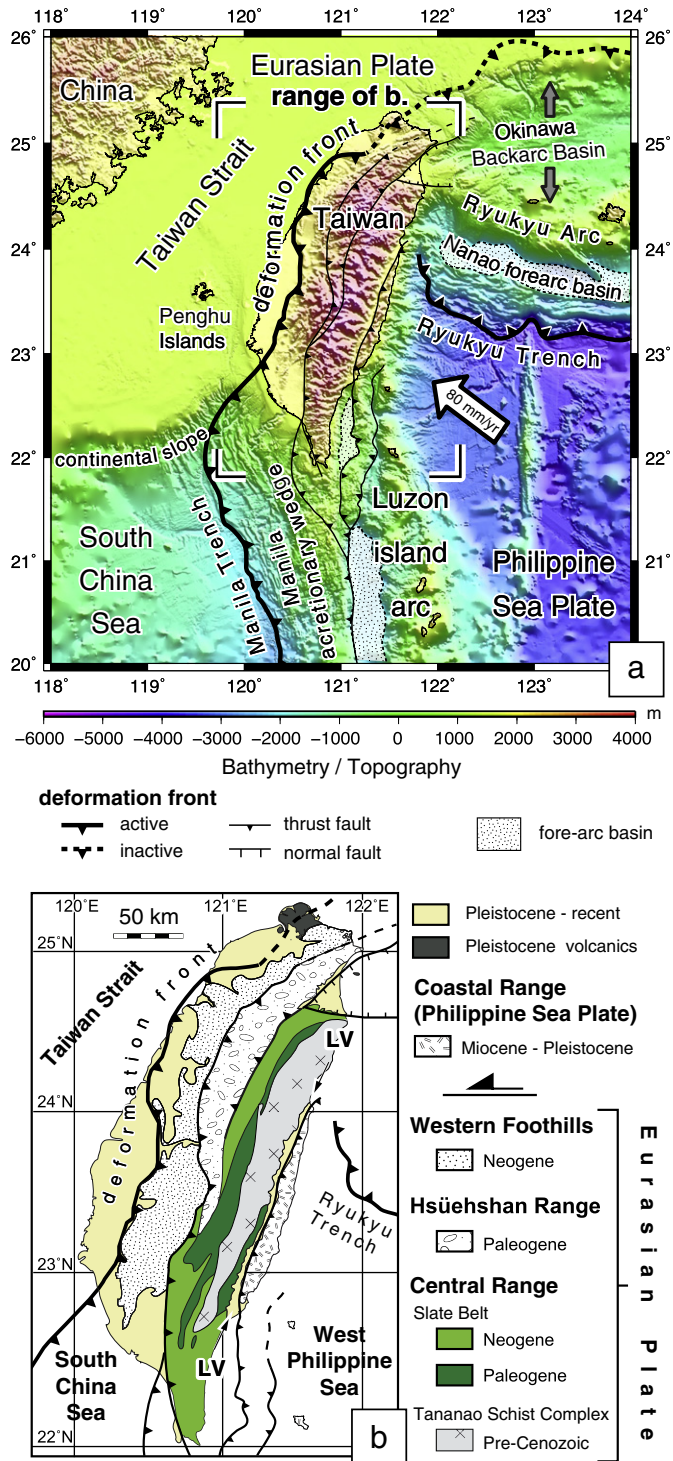


Fig. 1. (a) Plate tectonic setting around the Taiwan–Luzon arc-continent collision. The transition from active to inactive deformation front in northern Taiwan is after Teng et al. (2001), its offshore continuation after Hsiao et al. (1998). (b) Simplified tectonic map of Taiwan. Converging arrows labeled 'LV' depict the Longitudinal Valley.

plate as it subducts underneath Eurasia at the Ryukyu trench. In addition, rollback and delamination of the subducting Eurasian slab operate under northern Taiwan, progressively deactivating the deformation front and triggering post-collisional magmatism. In combination, these observations support a model of progressive subduction polarity reversal propagating along the Eurasian continental margin.

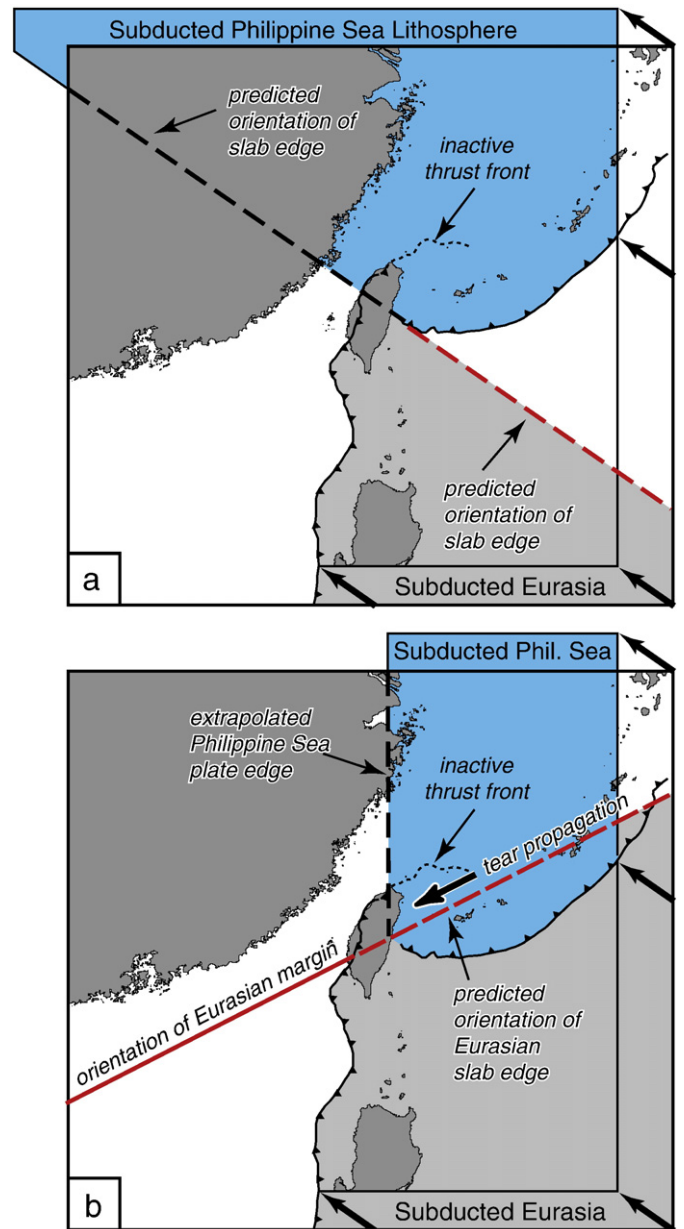


Fig. 2. Models of subduction polarity reversal proposed for Taiwan. (a) Instantaneous polarity reversal at a trench–trench transform, and (b) progressive polarity reversal by propagating a tear in the Eurasian lithosphere along the edge of the continent. See text for references.

2. Tectonic setting

The collision between the passive margin of the Eurasian plate and the Luzon island arc of the overriding Philippine Sea plate formed an actively growing mountain belt since about 4 to 5 Ma (Chang and Chi, 1983; Chi et al., 1981; Suppe, 1984; Yu and Chou, 2001). The parts emerging above sea level form the island of Taiwan (Fig. 1a and b). To the south of Taiwan, Eurasian lithosphere subducts underneath the Philippine Sea plate. This geometry is inherited from the intraoceanic subduction of South China Sea lithosphere underneath the Philippine Sea plate, which commenced after the end of spreading in the South China Sea at around the early Middle Miocene (c. 16 Ma; Taylor and Hayes, 1983; Sibuet et al., 2002). Intraoceanic subduction still prevails south of Taiwan along the Manila trench (e.g., Malavieille et al., 2002; McIntosh et al., 2005; Reed et al., 1992). Teleseismic p-wave tomography suggests c. 800 km of South China Sea lithosphere

subducted underneath the Philippine Sea plate (Fig. 6 in Lallemand et al., 2001; Li et al., 2008). The estimated Philippine-Eurasia plate convergence velocity of 70–90 mm/yr in a northwest direction (305°, Seno, 1977; Yu et al., 1997) implies a minimum of 10 Ma of plate convergence, corroborating the estimates on the onset of intraoceanic subduction. To the northeast of Taiwan, the Philippine Sea plate subducts underneath the Eurasian plate along the Ryukyu trench (Fig. 1). The highly oblique subduction of the north-dipping Philippine Sea slab (towards 305°, Seno, 1977) is accompanied by westward propagation of the Okinawa back-arc trough and southward retreat of the Ryukyu trench (Letouzey and Kimura, 1986), likely controlled by southward rollback of the subducting Philippine Sea plate (Sibuet and Hsu, 2004; Teng, 1996; Fig. 1). The westward propagation of the Okinawa back-arc trough led to extensional reactivation of compressional structures in the northeastern part of the Taiwan fold-and-thrust belt (Teng et al., 2001), leaving the deformation front in northernmost Taiwan and its offshore continuation to the northeast inactive (Hsiao et al., 1998; Wageman et al., 1970; Fig. 1a and b).

2.1. Constraints on the plate interface

Both the eastward dipping Eurasian slab and the northward dipping Philippine Sea slab are unambiguously imaged by a large number of earthquakes illuminating both Wadati-Benioff zones (Chou et al., 2006; Kao and Rau, 1999; Kao et al., 2000; Kim et al., 2005; Ma et al., 1996; Rau and Wu, 1995; Tsai, 1986; Tsai et al., 1977; Wu et al., 1997, 2009a). However, north of 23°N under central Taiwan there is little seismicity at depths >50 km (Lin and Roecker, 1993; Ma and Liu, 1997; Rau and Wu, 1995; Roecker et al., 1987; Tsai, 1986). This renders earthquake distribution useless for imaging the plate interface in an area that is very critical for understanding the mechanism of subduction reversal. The absence of deep earthquakes north of 23°N was attributed to a larger amount of continental lithosphere subducted (Lin, 2002) and hence insignificant slab dehydration (Chen et al., 2004). Alternatively, it has been proposed that lower yield stresses (Ma and Song, 2004) and a shallower depth of the 350 °C isotherm, corresponding to the brittle-ductile transition (Lin, 2000), could explain the absence of deep earthquakes under Central Taiwan.

There is seismological evidence for an east-dipping slab underneath Central Taiwan despite the absence of deep earthquakes. Chen et al. (2004) noticed an azimuthal dependence of the amplitude patterns of teleseismic p-wave arrivals, which they attributed to an east-dipping, 400–500 km long aseismic slab of continental lithosphere under Central Taiwan. An azimuthal dependence of amplitudes and travel times of direct p-waves and those refracted at the Moho was also observed for local earthquakes (Lin, 2009), compatible with an eastward subducting Eurasian slab under central Taiwan. Using P-wave tomography from both local and teleseismic arrivals, Wang et al. (2006, 2009) also imaged an eastward dipping Eurasian slab underneath Taiwan, steepening at about 24°N.

2.2. The Moho underneath Taiwan

Numerous studies aimed at determining depth and geometry of the Moho discontinuity beneath Taiwan, based on various data and methods: gravity (Yen et al., 1998), Pn studies (Chen et al., 2003; Liang et al., 2007; Ma and Song, 1997), P- and S-wave tomography (Chen and Shin, 1988; Cheng, 2009; Kim et al., 2005, 2006; Ma and Liu, 1997; Ma et al., 1996; Rau and Wu, 1995; Roecker et al., 1987; Wu et al., 2007), active source wide-angle seismics (McIntosh et al., 2005; Yeh et al., 1998), travel time inversion of passive mantle reflections (PmP, SmS and SmP, Lin, 2005; PmP, Hsu et al., 2011) and receiver functions (Kim et al., 2004; Wang et al., 2010). The different studies produced at times conflicting results. From modeling of gravity data, Yen et al. (1998) concluded that the Eurasian Moho has a depth of

26–28 km under the western Coastal Plain and Western Foothills (Fig. 1b), reaching 33 km beneath the Central Range. Pn studies placed the foreland Moho at a depth of about 35–40 km, and at 45 km under the Central Range (Chen et al., 2003; Ma and Song, 1997). However, the Pn method generally assumes that the Moho surface is planar; therefore it is of limited applicability in Taiwan, where reflectors are strongly dipping. In tomography, a 3D gridded model is used to interpolate the velocity structures and the depth of the Moho is usually estimated from an arbitrarily assigned Vp contour (e.g., Kim et al., 2005; Wu et al., 2007). The average Moho depth estimated from tomography is 30–35 km below western Taiwan (e.g., Ma et al., 1996), deepening to 50–70 km underneath the Central Range (e.g., Kim et al., 2005; Ma et al., 1996; Wu et al., 1997). This approach also has its shortcoming in that it disregards the possibility of lateral velocity variations at Moho depth. Wide-angle deep seismic profiling may provide information on thickness and velocities of the crust through direct, PmP and Pn waves. Currently, there are only two such transects across Taiwan (McIntosh et al., 2005; Yeh et al., 1998), which is insufficient to retrieve the Moho structure at greater distance from the transects. Yeh et al. (1998) suggested a Moho depth of about 40 km below the Coastal Plain and Western Foothills, deepening to 56 km below the Central Range and substantially shallowing towards east. From passive seismic mantle reflections (PmP, SmS and SmP) recorded by a linear seismic array in the Western Foothills, Lin (2005) inferred an eastward deepening Moho, reaching at least 50 km depth beneath the Longitudinal Valley. Receiver function studies make use of teleseismic arrivals with high incident angles that convert part of their energy into new phases at distinct velocity interfaces within the lithosphere. Such studies have the advantage that the incoming rays actually penetrate the discontinuities one aims to model. Using the P-to-S converted phase, Wang et al. (2010) constrained the depth of the Moho underneath Taiwan to range between 11 and 53 km.

Despite methodological differences, most studies revealed a progressive deepening of the Eurasian Moho from the foreland towards the Central Range, shallowing again underneath the Coastal Range to about 20 km depth (Cheng, 2009; Kim et al., 2006; Liang et al., 2007). Numerous studies have also demonstrated a systematic eastward offset of the deepest position of the Moho with respect to the topographic crest of the mountain range under the Central Range, suggesting that the orogen has not yet attained isostatic equilibrium (Kim et al., 2004; Lin, 2005; Yeh et al., 1998). However, most studies depicted the Moho merely along few 2D transects. Given the complex plate tectonic configuration around Taiwan, it is unclear which of these transects can be considered representative. Likewise, studies relying on arrays with larger coverage, depicting a contiguous Moho surface under Taiwan (e.g., Hsu et al., 2011; Wang et al., 2010) neglect the fact that the Eurasian and Philippine Sea plates are juxtaposed along a plate interface, across which each Moho is offset. Therefore, they presumably do not adequately portray all complexities.

3. Methods and results

The aim of the present study was to define 3D geometries of all crust–mantle boundaries (i.e., both the Mohos and the plate boundary) in the Taiwan–Luzon arc collision zone, addressing particularly the issue how their geometry is affected by the subduction polarity reversal. We made use of several datasets that offer increased spatial resolution in this region. Wu et al. (2007, 2009b,c) obtained a 3D model of the Vp, Vs and Vp/Vs structure of Taiwan by combining a large dataset of P- and S-wave arrival times of local earthquakes from the Taiwan Strong Motion Instrumentation Program (TSMIP) with those of the Central Weather Bureau Seismic Network (CWBSN), permanent stations of the Japan Meteorological Agency as well as temporarily deployed ocean bottom seismometers (OBS). This dataset includes more than 800 stations throughout the island as well as in offshore areas. It improved the source to station path coverage and provided much better

constraints and resolution on the velocity structure. It also provided constraints to conduct 3D relocations of earthquakes (Wu et al., 2008a) as well as focal mechanisms determination (Wu et al., 2008b). For the purpose of this study, we combined the above datasets with layered P-wave velocity models that offered additional insights on the crustal velocity structure.

3.1. Layered P-wave velocity (1D) modeling with a genetic algorithm

3D tomographic velocity models do not contain information on any crustal discontinuities across which seismic velocities change. In order to model horizontally layered crust containing such discontinuities, we made use of the fact that P-wave travel times at each seismic station carry information about the crust below it. We hence determined one-dimensional layered velocity models of the crust using P-wave travel times at each station (termed 1D models from now on). The 1D models provide information about the change of Vp with depth, from which the crust–mantle boundary depth at a given location can be estimated. We used P-wave arrivals from the CWBSN catalog, which employs 71 tele-metered stations with 3-component S-13 Teledyne Geotech seismometers (Wu et al., 2008a, Fig. 3). The P-wave travel times underwent a 3D earthquake relocation process (Wu et al., 2008a). In order to offer velocity information beneath each station, we used only the P-wave travel times of events with an epicentral distance equal to or less than two times the focal depth (Fig. S1a in the supplementary dataset to this article). The P-wave travel times were assigned values from 0, 1, 2, to 3, with 0 = good and 3 = poor (Lee and Lahr, 1975) and used with a

weighting of 1.5, 1.0, 0.5 and 0.125, respectively, for calculating travel time fit. In total, 52 stations with more than 2000 P-wave travel times per station were used (Fig. 3 and Table 1). Stations that do not meet this requirement are usually at the periphery of the network (Fig. 3).

A genetic algorithm was used for determining 1D models. The genetic algorithm is a technique inspired from the biological process of evolution by means of natural selection and has become an established tool for search and optimization problems. Proposed by Holland (1975), it had developed to approach nonlinear optimization (e.g., Goldberg, 1989). It has been applied to numerous scientific problems including seismology (cf. Wu et al., 2008b and references therein). The genetic algorithm adopted in this study is that of Goldberg (1989). The algorithm involves three operators of the

Table 1

Parameters of the CWBSN stations and depths to the crust–mantle boundary determined by the 1D models.

Station	Latitude (°N)	Longitude (°E)	Elevation (m)	Readings	Residual ^a (sec)	CMB ^b depth (km)	Vp at Moho (km s ⁻¹)
ALS	23.508	120.813	2413	24449	0.0703	47.1	7.78
CHK	23.098	121.373	34	12312	0.1037	28.8	7.73
CHN1	23.185	120.529	360	11377	0.1017	39.2	7.90
CHN2	23.532	120.474	45	6856	0.0546	37.9	7.72
CHN4	23.351	120.594	205	10625	0.0645	49.0	7.91
CHN5	23.597	120.677	840	15796	0.0589	48.9	7.67
CHN8	23.347	120.223	6	2038	0.1241	28.9	7.77
CHY	23.496	120.433	27	8333	0.0542	28.7	7.60
EAS	22.381	120.857	445	3253	0.1959	44.3	7.67
ECL	22.596	120.962	70	5131	0.2040	32.3	7.73
EHC	24.265	121.740	11	4209	0.1139	58.1	7.75
EHY	23.504	121.328	237	7918	0.2099	28.8	7.60
ELD	23.187	121.025	1040	8094	0.1055	31.6	7.56
ENA	24.426	121.749	113	19938	0.1202	70.9	7.85
ENT	24.637	121.574	280	16477	0.1537	59.0	7.84
ESL	23.812	121.442	178	14129	0.1574	30.1	7.81
HWA	23.975	121.614	16	10110	0.1017	32.1	7.81
ILA	24.764	121.756	7	3872	0.1440	45.8	7.57
NNS	24.438	121.381	1140	11259	0.1557	67.7	7.93
NSK	24.674	121.367	682	12936	0.1240	40.8	7.68
NST	24.630	121.009	164	9495	0.1351	42.1	7.53
NSY0	24.415	120.769	311	7461	0.0843	51.4	7.73
NWF	25.072	121.781	765	4996	0.1669	38.4	7.72
SCZ	22.370	120.628	74	3555	0.1214	42.0	7.90
SGS	23.080	120.591	278	9865	0.0987	40.3	7.57
SML	23.882	120.908	1015	17679	0.0972	60.5	7.60
SSD	22.744	120.640	148	8026	0.0875	45.9	7.75
STY	23.161	120.766	640	13463	0.0930	58.4	7.85
TAW	22.356	120.904	8	2708	0.2082	41.7	7.86
TCU	24.146	120.684	84	7500	0.1214	47.8	7.70
TTN	22.752	121.155	9	3425	0.1589	77.0	7.68
TWA	24.978	121.592	260	6015	0.1575	37.9	7.68
TWB1	25.007	121.997	130	7361	0.1461	40.6	7.69
TWC	24.608	121.860	20	21684	0.1421	56.9	7.77
TWD	24.081	121.605	30	19170	0.1113	37.3	7.92
TWE	24.718	121.683	20	16349	0.1485	43.8	7.88
TWF1	23.351	121.305	260	10360	0.1773	30.9	7.93
TWG	22.818	121.080	195	12380	0.1637	26.8	7.58
TWL	23.264	120.502	590	10766	0.0930	33.8	7.58
TWM1	22.822	120.431	340	2749	0.1286	33.7	7.59
TWQ1	24.347	120.781	231	12056	0.0822	31.6	7.51
TWS1	25.102	121.423	60	4781	0.1635	27.1	7.55
TWT	24.252	121.184	1510	9719	0.1045	65.6	7.86
TWT0	24.252	121.184	1510	5826	0.1785	59.8	7.86
TWU	24.876	121.542	330	3362	0.1227	41.0	7.80
TWY	25.273	121.607	20	2118	0.1647	36.1	7.54
TYC	23.905	120.870	20	15295	0.1140	54.6	7.68
WDT	23.754	121.141	2550	7475	0.1522	32.8	7.61
WGK	23.685	120.570	75	7750	0.0670	46.4	8.00
WHF	24.144	121.273	148	14318	0.1980	64.0	7.99
WNT	23.877	120.693	110	8441	0.0953	39.1	7.66
WTP	23.244	120.622	560	10397	0.0874	48.2	7.98
YUS	23.487	120.959	134	13849	0.0793	68.1	7.94

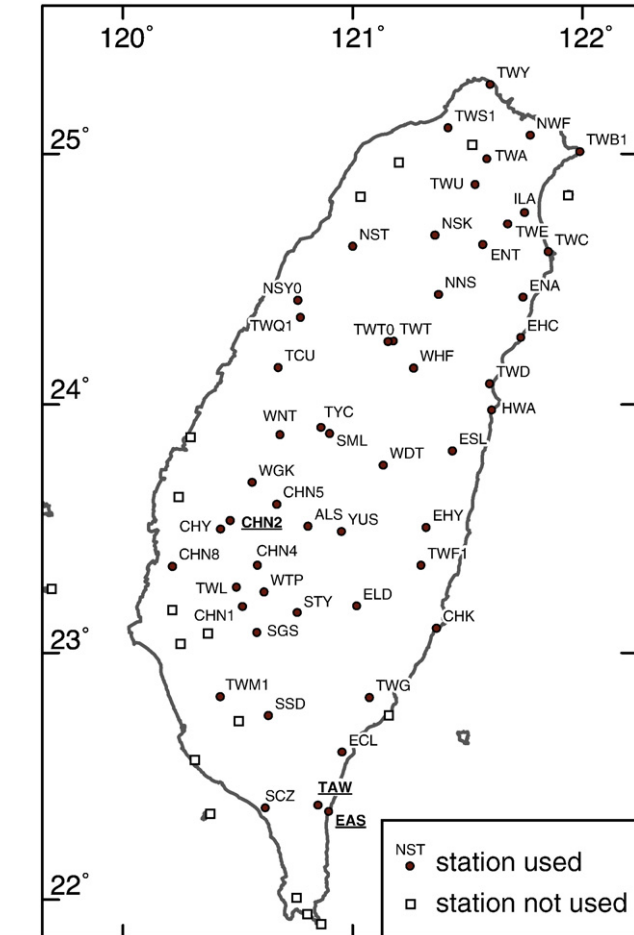


Fig. 3. Distribution of CWBSN seismic stations used for obtaining layered Vp (1D) models. Bold, underlined stations are those shown in Fig. 4.

^a Average and weighted travel time residuals.

^b CMB = crust–mantle boundary.

natural selection, namely the reproduction, crossover and mutation. A FORTRAN computer program was used for the simultaneous determination of V_p and layer thickness in the 1D models. For each model a maximum of 50 layers is allowed. Each parameter of V_p and thickness is designed in binary code with 10 digits. In total, each model has 1000 digits. In considering large searching ranges, a high mutation rate at 69% is used in this study based on a previous one (Wu et al., 2008b). Reproduction rate is given for 1% and 30% for crossover. We randomly produced the initial models and a 1D model routinely used by the CWBSN for earthquake localization (Chen and Shin, 1988) is used as one of the initial models for quick convergence. Fig. S1b shows the reduction of averaged and weighted travel time residuals versus genetic algorithm generations. The travel time residuals are drastically reduced after the first 100 iterations (or generations, Fig. S1b). After c. 500 generations, further residual reduction becomes insignificant. Hence, the models were terminated after 1000 generations (Fig. S1b).

In total, 52 1D models were determined. The crust–mantle boundary was defined at a depth where $V_p \geq 7.5 \text{ km s}^{-1}$ was first reached in the layered model. This value is in agreement with geophysical definitions of a seismic Moho (e.g., Giese et al., 1999; Jarchow and Thompson, 1989; Mooney, 2007) and represents a global average on the lower bound of P-wave velocities of most ultramafic rocks (Christensen and Mooney, 1995; Press, 1966). Fig. 4 shows the 1D models determined from stations CHN2, TAW, and EAS. Of all models, CHN2 and TAW show the minimum and maximum residuals between calculated and observed travel times, respectively. Generally, the 100 best models are close to the best model, with station EAS showing the poorest fit. Table 1 and Fig. S2 show the crust–mantle boundary depth determined with this approach at all 52 stations. Fig. 5 shows a contour map of the crust–mantle boundary derived exclusively from the 1D models, i.e. without considering a plate boundary. Its depth ranges between 50 km beneath the Central Range (at a latitude of about 23°N) and 70 km south of the Ilan plain (at a latitude of 24.5°N). In western Taiwan and beneath the Coastal Range it shallows to c. 30 km. Fig. S3 shows the variation of V_p at the crust–mantle boundary depth as determined from the 1D models. The misfit (L1 norm) of the travel times (i.e., the travel time residuals of each

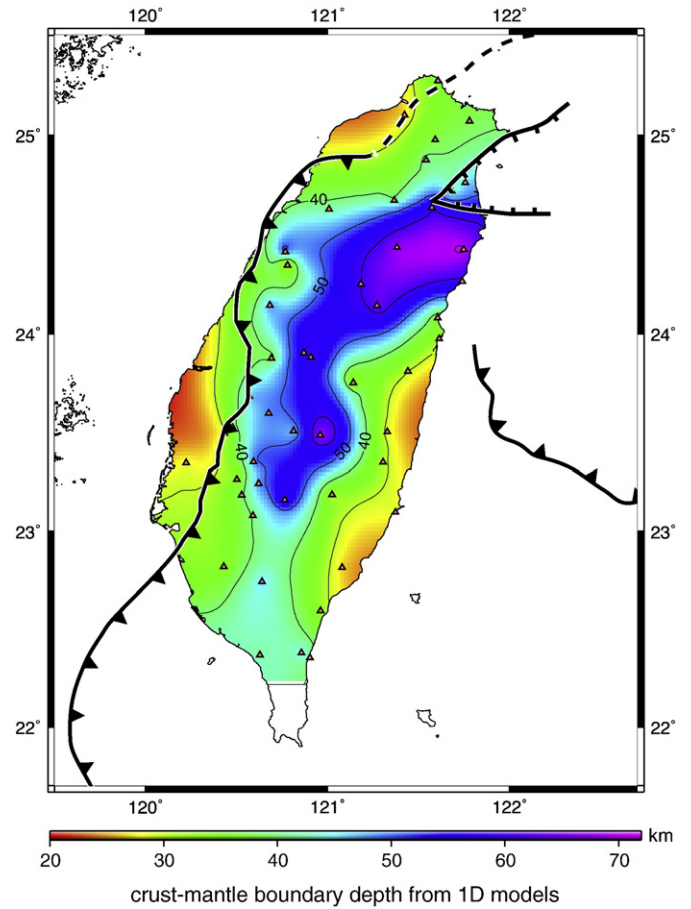


Fig. 5. Crust–mantle boundary contour map constrained solely from 1D models, without consideration of the plate tectonic association. Major tectonic lines in this and all consecutive maps correspond to Fig. 1.

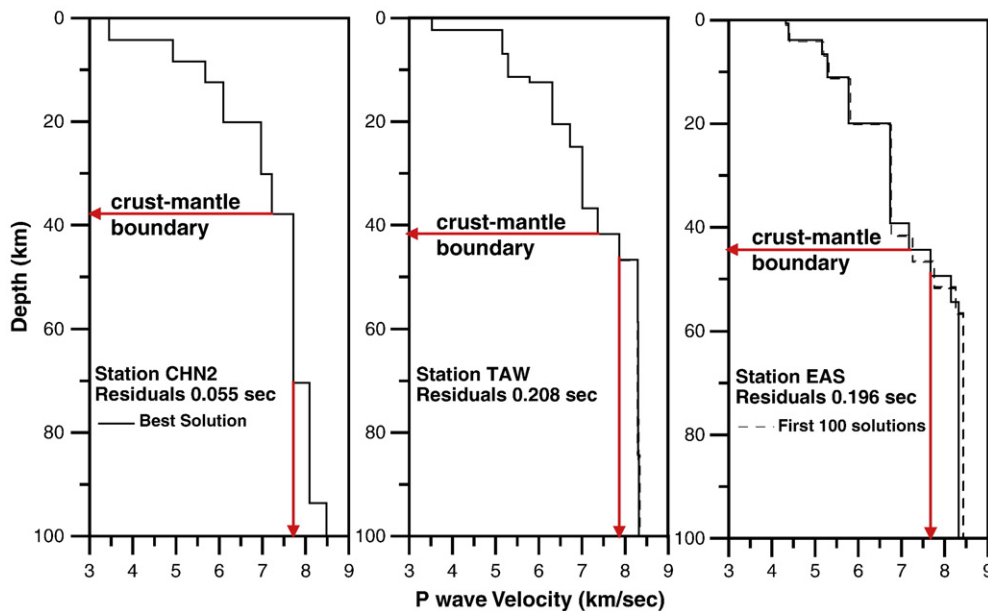


Fig. 4. 1D model results for three stations (see Fig. 3 for their locations). Stations CHN2 and TAW gave the smallest and largest travel time residuals after 1000 iterations. Station EAS yielded the largest misfit in calculated velocities between the first 100 model generations and the final iteration. The crust–mantle boundary was arbitrarily defined at a depth at which V_p reaches $\geq 7.5 \text{ km s}^{-1}$ in the layered model. The solid line depicts V_p determined by the best model; the dashed lines show the V_p range obtained by the 100 best models.

station, Fig. 6) range from 0.055 s (station CHN2) to 0.208 s (station TAW, see Table 1).

If interpreted as the Moho, the general pattern in Fig. 5 agrees with previous studies (Section 2) up to the point of portraying a shallower Moho underneath both western Taiwan and the Coastal Ranges. However, Fig. 5 is not yet an adequate representation of the Moho, because the 1D modeling approach does not take account of the plate interface separating the Eurasian and Philippine Sea plates. Fig. 5 suggests contiguous contours, where we expect the plate boundary between Eurasian and Philippine Sea plates (compare Figs. 1a and 5). We suspect that the actual Moho geometry implies the existence of two topologically unconnected surfaces separated by the plate interface. This required a more refined approach that combined 1D models, velocity information from tomography and earthquake distribution.

3.2. 3D contouring using local earthquake tomography

The tomographic dataset of Wu et al. (2007) was converted into a 3D volume for treatment in gOcad, a software for advanced structural modeling (Mallet, 1992). The 3D volume contained the properties V_p , V_s , V_p/V_s and the number of P-readings (corresponding to the ray coverage per tomographic cell). The tomographic cells are spaced by 7.5 and 12.5 km in the horizontal plane for all onshore parts of Taiwan, and 20×20 km in the offshore areas. The vertical cell spacing ranges from 2 km between 0 and 6 km depth to 60 km between 140 and 200 km depth (Wu et al., 2007). Animation S1 (see supplementary data to this article) shows horizontal slices through this tomographic dataset, depicting V_p together with the seismicity within the corresponding depth slice (dataset of Wu et al., 2008a). We mapped points

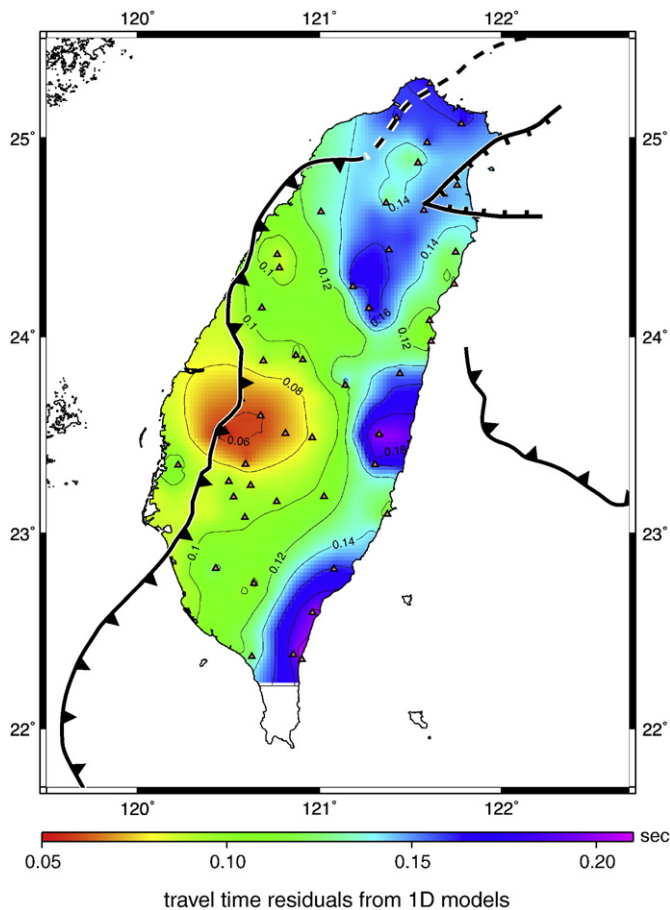


Fig. 6. Travel time residuals at the depth of the crust–mantle boundary constrained from 1D modeling.

of constant $V_p = 7.5 \text{ km s}^{-1}$ onto a total of 68 vertical cross sections through the tomographic dataset. The sections were oriented N110°E, parallel to the local coordinate frame of the tomographic dataset, and regularly spaced at 10 km. We thus obtained sections through every tomographic cell. Signals with a wavelength below the dimension of the tomographic cells were disregarded in order not to pick potential artifacts introduced by the interpolated tomographic dataset. Also, we restricted our interpretations to areas with a ray coverage of at least 500 readings per tomographic cell. This ensured that we did not merely pick information from the horizontally layered input velocity model. With this approach we defined several point sets in 3D. By triangulation, each point set was subsequently converted into a surface corresponding to a constant value of $V_p = 7.5 \text{ km s}^{-1}$. These triangulated ‘isovelocity’ surfaces are all topologically disconnected. In the following, we describe how we attributed these surfaces to the Eurasian and Philippine Sea plate Moho as well as to the plate interface separating them. The final geometries of the 3D surfaces are illustrated by Animations S2, S3 and S4 (supplemental material to this article).

3.2.1. Plate interface

The first isovelocity surface discussed represents the plate interface, which separates the Eurasian lower crust ($V_p < 7.5 \text{ km s}^{-1}$) from the overlying Philippine Sea plate mantle lithosphere ($V_p \geq 7.5 \text{ km s}^{-1}$, color-coded contours in Fig. 7a). A $V_p = 7.5 \text{ km s}^{-1}$ contour could only be mapped at depths greater than c. 15–20 km. We nevertheless extended the isovelocity surface up to the topographic surface, making use of the fact that the plate interface is exposed in the Longitudinal Valley (‘LV’ in Fig. 1b). This valley hosts the suture separating Eurasia-derived units in the eastern Central Range from the arc- and forearc-derived units in the Coastal Range (Fig. 1b). In the southeast, the plate interface dips towards east (Fig. 7a). At depths greater than 50 km, it coincides with an east-dipping Benioff zone underneath southeastern Taiwan (Wu et al., 2008a; Fig. 7b). Assuming a thickness of the overlying Philippine Sea plate of c. 100 km, the contoured surface is no longer a plate interface at depths greater than 100 km, but represents the top of the subducting Eurasian slab that is directly juxtaposed against asthenosphere. However, this could not be determined from the V_p tomography. Towards north, the plate interface steepens progressively until it becomes vertical at 23.7°N. From there it continues northward in an essentially vertical orientation, until the limit of the tomographic model at the northern tip of Taiwan inhibited further mapping. North of the Ryukyu trench (i.e., north of 24°N), this plate interface abuts the western edge of the north-dipping Benioff zone, which is confined to the subducting Philippine Sea plate (black contours in Fig. 7a). This Benioff zone (Fig. 7b) represents the plate interface between the Eurasian and Philippine Sea plates, but with reversed polarity compared to above. The contours of the north-dipping plate interface were constructed by fitting a regression surface through the average distribution of earthquakes within the Benioff zone (dataset of Wu et al., 2008a), i.e., independent of the tomography. Topologically, the color-coded and black contours (Fig. 7a) hence depict the bottom and top of the Philippine Sea plate, respectively (and not one and the same overturning plate interface).

3.2.2. Eurasian and Philippine Sea plate Mohos

In addition to the triangulation, the isovelocity surfaces representing the Eurasian and Philippine Sea plate Mohos (Figs. 8 and 9) underwent a smoothing procedure using the discrete smooth interpolation technique (Mallet, 1992) with 5 iterations. This technique allows using a set of ‘control points’ to which the depth of the triangulated surface will be adjusted during the interpolation, depending on how much weighting is put to these constraints. Weighting is controlled by an arbitrarily chosen fitting factor; the lower this factor, the less weight is given to the constraints. In our case, the crust–mantle boundary depths obtained from the 1D models

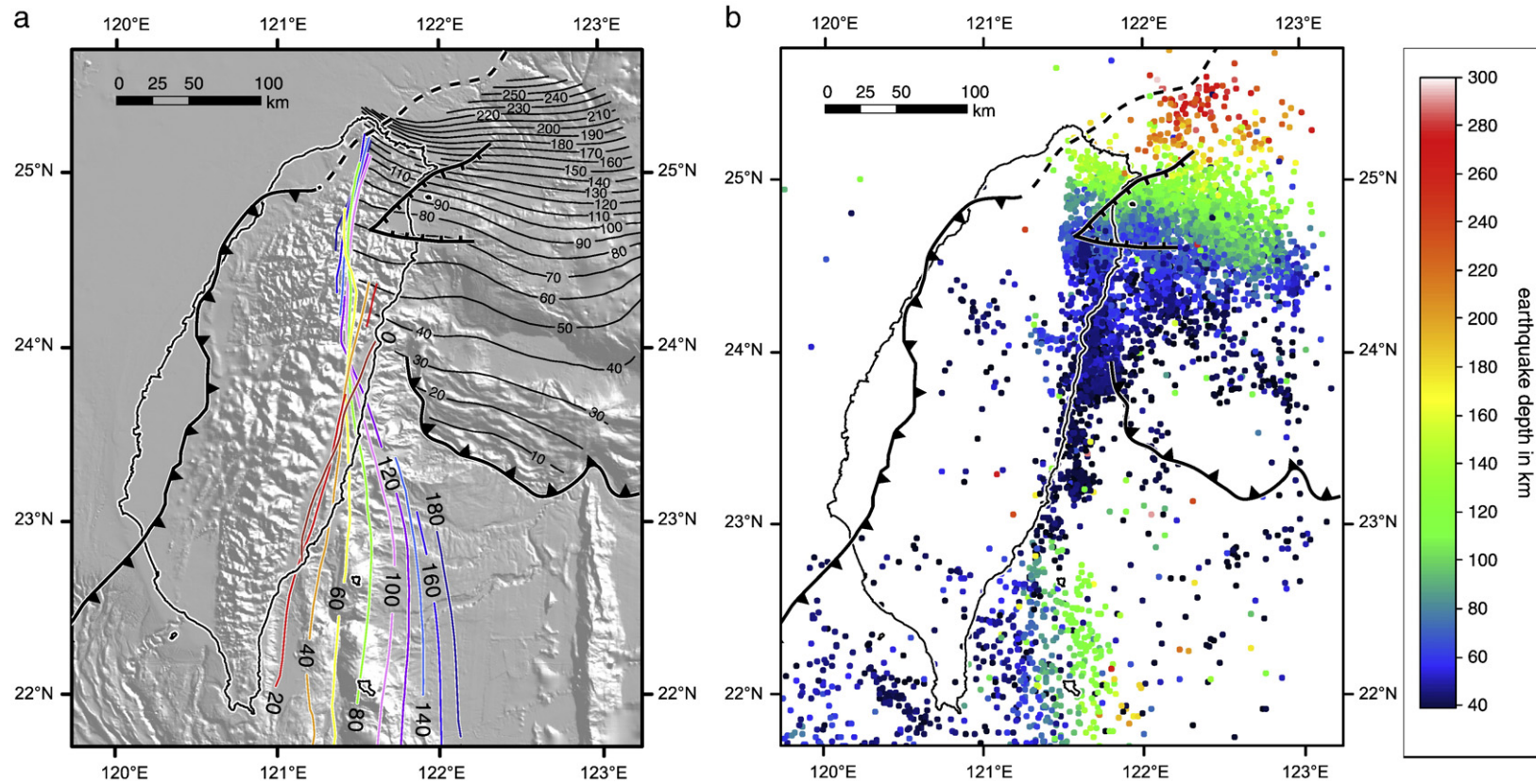


Fig. 7. (a) Color-coded contours indicate an isovelocity surface of $V_p = 7.5 \text{ km s}^{-1}$ from the tomographic grid, corresponding to the plate interface separating the Eurasian lower crust ($V_p < 7.5 \text{ km s}^{-1}$) from the Philippine Sea lithosphere ($V_p \geq 7.5 \text{ km s}^{-1}$). At depths greater than c. 100 km the plate interface continues as the top of the subducting Eurasian slab. The surface changes its dip direction along-strike from east-dipping in the south to essentially vertical in the north. The 0 km contour follows the Longitudinal Valley. Black contours depict the north-dipping Philippine Sea plate slab, constructed from fitting a regression surface through the Benioff zone (shown in b). Contours in this and all consecutive maps are labeled in km. (b) Earthquakes with $M \geq 3.0$ and a hypocenter depth $\geq 40 \text{ km}$ (Wu et al., 2008a). The clear-cut western edge of seismicity is confined to the northward dipping Philippine Sea plate and abuts the plate interface as constrained from tomography.

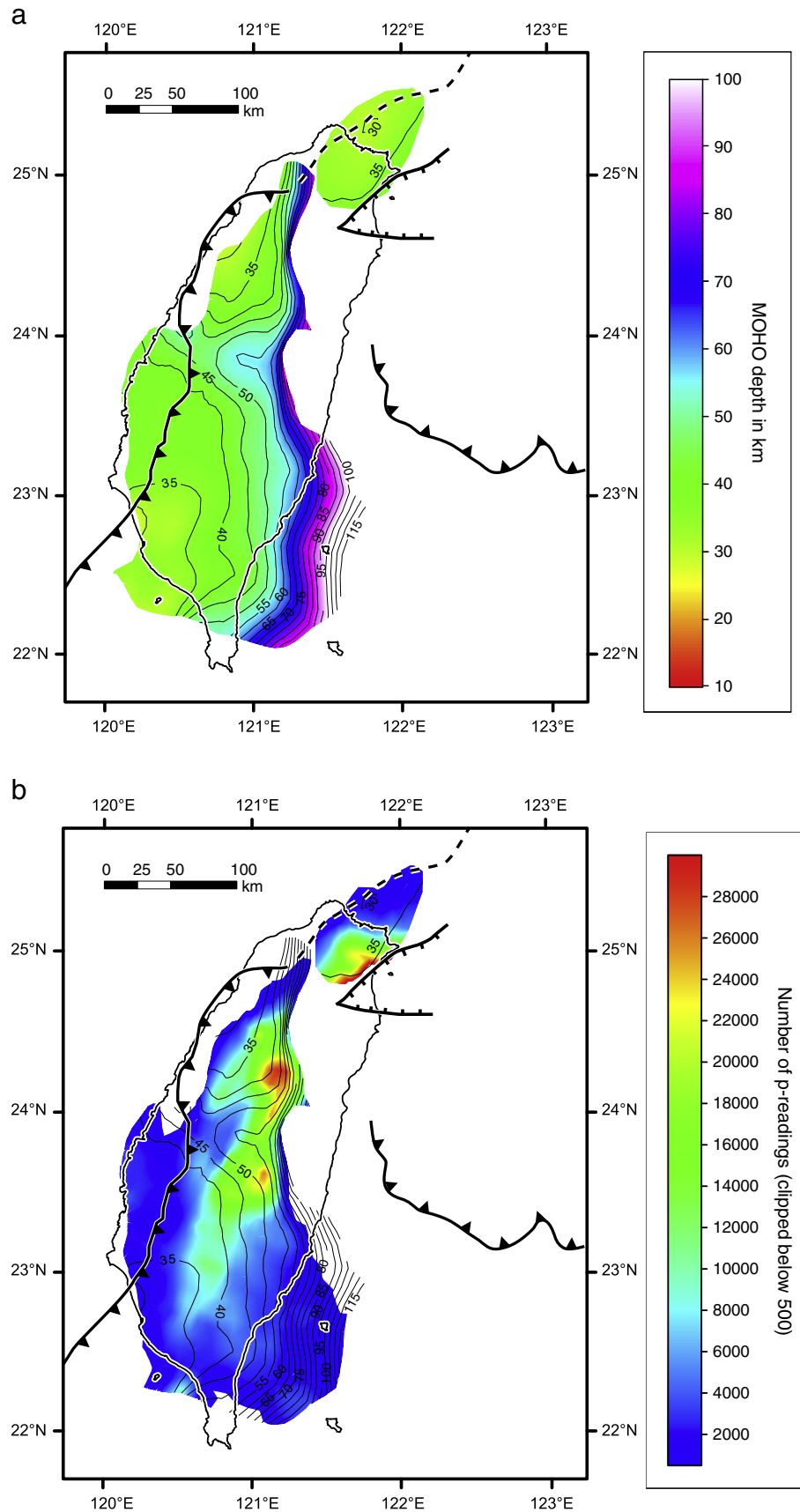


Fig. 8. Map of the Eurasian Moho, (a) color-coded for depth, (b) color-coded for the number of readings of p-wave arrivals (transparent where <500), and (c) same as in (a), additionally showing the “mismatch”, i.e. the vertical distance between the interpolated surface and the 1D model constraints.

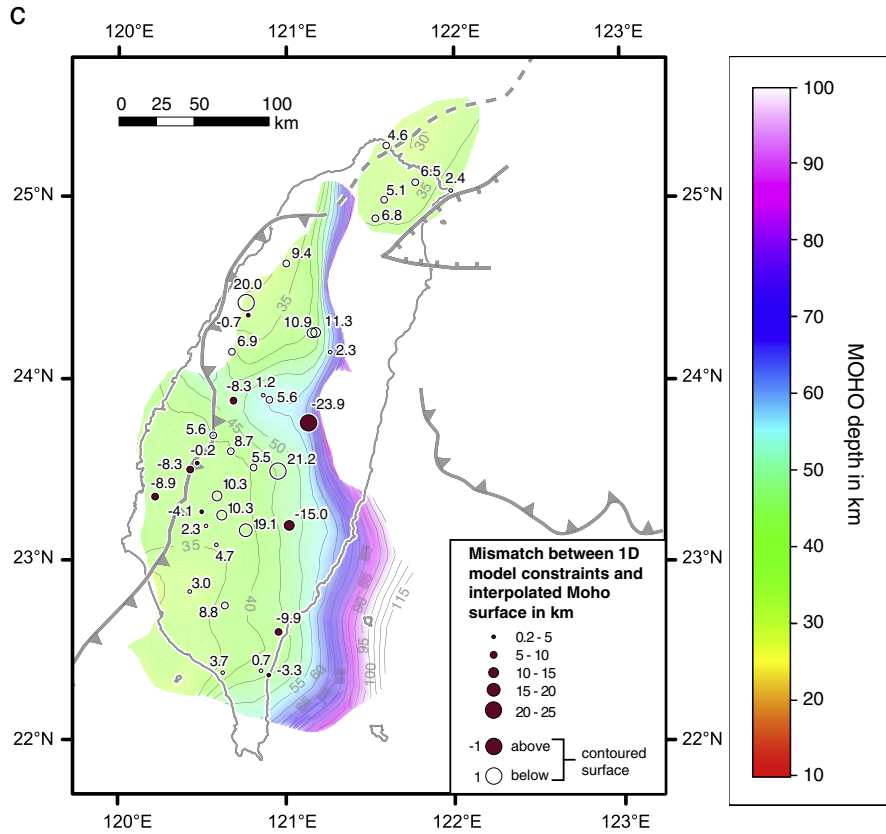


Fig. 8. (continued).

served as control points, as described in the following. For this purpose, it is pivotal to remind ourselves that these models provide only first-order estimates at which depth a crust–mantle boundary may be located; they do not distinguish the nature of this boundary (i.e., Moho or plate interface). Therefore, we assigned each of the 1D model constraints on the depth of the crust–mantle boundary (Fig. 5) to either (a) the Eurasian Moho, (b) the Philippine Sea Moho or, (c) the plate interface separating the Eurasian crust and the Philippine Sea mantle lithosphere, depending on their position with respect to the inferred plate boundary (Fig. 7a; see Fig. S4 and Table S1 for the resulting assignments). Stations assigned to category c were not used as control points for constraining the plate interface (Fig. 7a) owing to its overall steep dip in vicinity of the stations. For the interpolation, we used an empirically derived fitting factor of 1, which, by experience, constrained the depth of the smoothed surfaces within a range of c. 10% of the initial isovelocity surfaces. A fitting factor higher than 1 minimized the vertical distance between triangulated surface and the 1D models (termed “mismatch” in the following), but introduced high-frequency roughness (or rugosity) to the interpolated surfaces, which we considered geologically not realistic. A surface with a minimized mismatch is shown for the Eurasian Moho (Fig. S5). It features a narrow N–S trending upward bulge under central Taiwan, in which the Moho shallows from 60 to 45 km depth before dipping eastwards (Fig. S5). Given the overall subduction setting of the Eurasian slab, this geometry is considered highly unlikely. Hence, for geological reasons we gave preference to smooth interpolated isovelocity surfaces that in places retained considerable mismatch over highly rugose surfaces with a minimized mismatch.

Two interpolated isovelocity surfaces are interpreted as the Eurasian Moho (Fig. 8a). In the western foreland, the Eurasian Moho is between c. 35 and 40 km deep. At the latitude of 24°N under Central

Taiwan, it exhibits a roughly E–W trending depression reaching c. 50 km depth. From about 121°E eastwards, the Eurasian Moho dips towards east underneath the upper plate. Northwards, the Moho steepens. A subhorizontal Moho, topologically disconnected from the one just described, is confined to northeastern Taiwan (Fig. 8a). Fig. 8b shows the contoured surfaces of Fig. 8a, color-coded for the number of p-readings at each point of the surface. This criterion shows qualitatively how particular areas of the surface are constrained by the input seismic data. Parts of the Eurasian Moho constrained by less than 500 readings are uncolored (Fig. 8b). The mismatch between the interpolated isovelocity surface and 1D models is depicted in Fig. 8c.

The interpolated isovelocity surface representing the Philippine Sea plate Moho lies east of the plate interface (Fig. 9a). It displays a NNE-trending crustal root associated with the deformed arc and fore-arc units of the Coastal Range. A few km east of Taiwan’s coast, this crustal root is at a depth of c. 30 km. To the west and east of it, the Philippine Moho shallows to 20–15 km depth. Along-strike northward, the root can be traced for almost 200 km. It deepens towards north underneath the Ryukyu trench, reaching 65 km at the limit of the contoured surface. Fig. 9b depicts the contoured surface of the Philippine Sea plate Moho, color-coded for number of p-readings. In order to account for the poor station coverage offshore eastern Taiwan (and hence lower tomographic resolution), we raised the lower threshold of p-readings at each point of the Philippine Sea plate Moho surface to 5000 (Fig. 9b). Fig. 9c shows the mismatch between the interpolated surface and 1D models.

4. Discussion

We first discuss the retained mismatch between the 1D models and interpolated isovelocity Moho surfaces before focusing on the

geometry of all mapped crust–mantle boundaries, comparing with previous studies. Subsequently, we discuss the possible tectonic significance of the travel time residuals from the 1D models, as well as

the crustal thickness of the Philippine Sea plate. Eventually, we discuss our data in the light of a model of progressive subduction polarity reversal underneath Taiwan.

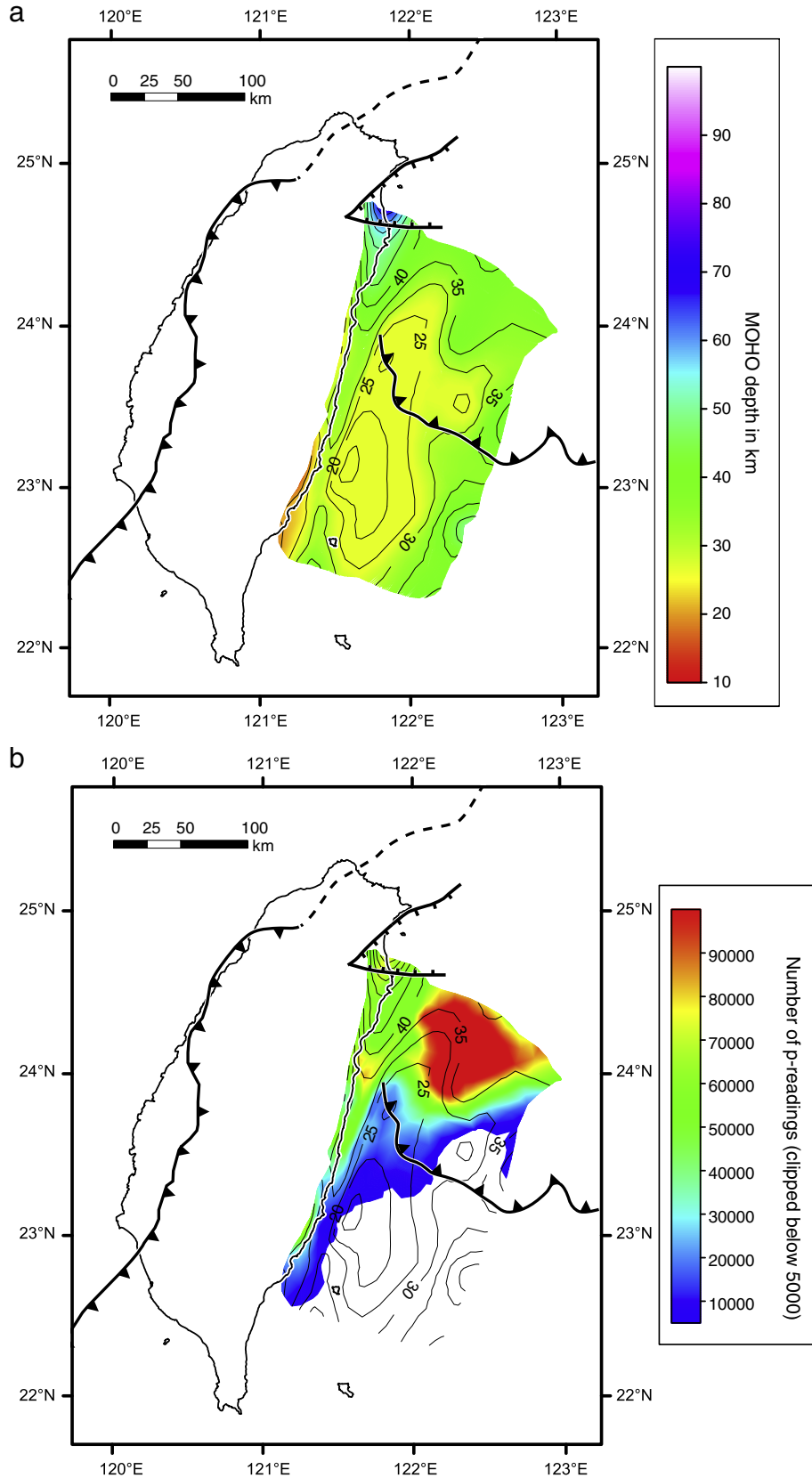


Fig. 9. Map of the Philippine Sea plate Moho, (a) color-coded for depth, (b) color-coded for the number of readings of p-wave arrivals (transparent where <5000), and (c) same as in (a), additionally showing the mismatch.

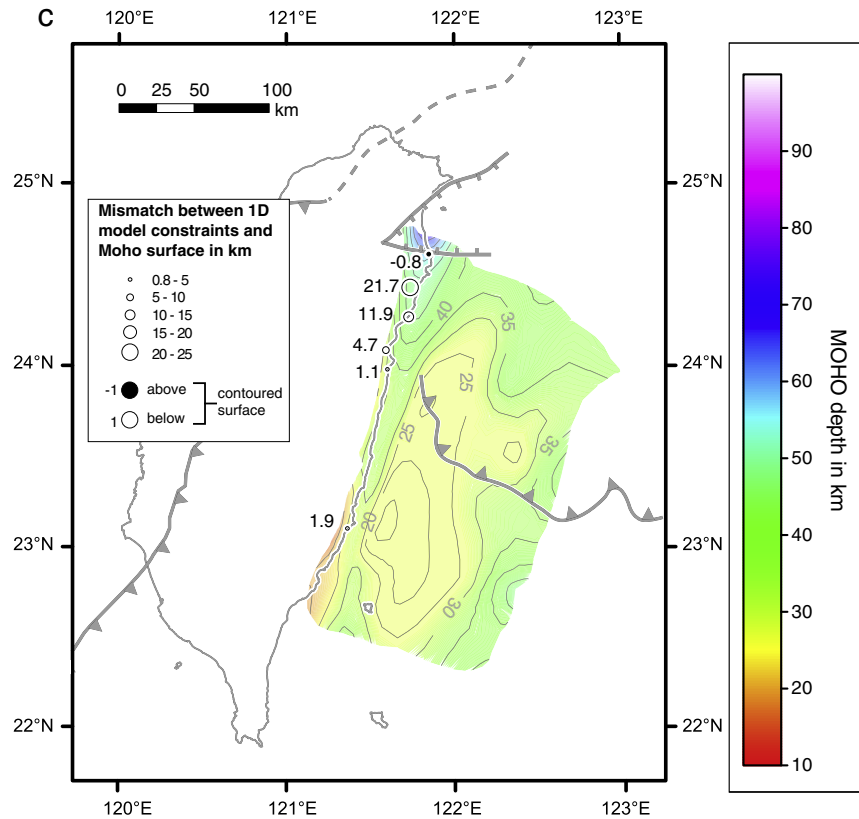


Fig. 9. (continued).

4.1. Mismatch between isovelocity Moho surfaces and 1D model constraints

Interpreting the Moho from tomographically defined isovelocity surfaces disregards the possibility of velocity variations introduced, e.g., by temperature (cf. Hyndman and Peacock, 2003, and references therein) or compositional changes in the lower crust. Under continents, compositional variations between lower crustal and upper mantle rocks may define a transitional zone up to 8 km thick rather than a sharp Moho (cf. Brown et al., 2009, and references therein). However, in the case of Taiwan we expected the Moho depth to vary by an order of magnitude more because of the subduction setting. Therefore we considered it viable to neglect Moho depth variations due to compositional changes. With this in mind, we now discuss possible reasons for the mismatch between 1D models and the interpolated isovelocity Moho surfaces.

32 1D models were used as constraints for the interpolated surface of the eastward-dipping Eurasian plate Moho (Fig. S4 and Table S1). Most of them constrain the Eurasian Moho deeper than the isovelocity surface mapped from tomography (Fig. 8c). A possible explanation for this is that Vp signals are assumed to arrive at the station at high incident angles, whereas the existence of dipping interfaces is not considered in these models. Velocity signals arriving from inclined reflectors are treated as if they emanated from horizontal reflectors directly underneath the station. This will tend to constrain the Moho surface at a given station deeper than it actually might be. This phenomenon is comparable to the problem of unmigrated reflection seismic data (cf., Stein and Wyssession, 2003).

Of the 32 constraints used for the Eurasian Moho, 11 show a mismatch of less than 5 km (from north to south and from west to east stations TWQ1, TYC, WHF, CHN2, TWL, CHN1, SGS, TWM1, SCZ, TAW and EAS). 11 show a mismatch between 5 and 10 km (stations

NST, TCU, WNT, SML, WGK, CHN5, ALS, CHY, CHN8, SSD and ECL). The models with a mismatch < 5 km show a sharp Vp contrast of ≥ 0.5 km s^{-1} at Moho depth. The remaining ten models exhibit a mismatch between 10 and 24 km, out of which seven constrained the Moho deeper than the modeled surface (stations NSY0, TWT0, TWT, YUS, CHN4, WTP and STY), while three models (stations WDT, ELD and TWG in the Central Range) lie above the surface modeled from tomography. Numerous of the models with a mismatch > 10 km show low Vp gradients at Moho depth below 0.5 km s^{-1} and/or large depth increments at sub-Moho depths (particularly stations WDT, YUS, STY and ELD that yielded the largest mismatch). This makes these models very susceptible to a large variability of Moho depth with only small changes in Vp. We presume that stations WDT and ELD, lying along-strike, represent outliers and that the actual Moho is deeper, i.e., where constrained from the tomography. Possibly, the layered models for these stations received Vp arrivals from the easterly adjacent plate interface. Alternatively, the Central Range in these areas could be underlain by lower crustal rocks with $Vp \geq 7.5$ km s^{-1} , representing, e.g., accreted eclogitic units. A distinction of eclogites and peridotites is not possible based on the Vp value (Christensen and Mooney, 1995; Press, 1966).

The subhorizontal Eurasian plate Moho in northeasternmost Taiwan was constrained by only six 1D models (stations TWA, TWY, TWS1, NWF, TWB1 and TWU). All models are characterized by a sharp Vp gradient at Moho depth and small depth intervals. This Moho is hence relatively well constrained. In the case of the Philippine Sea plate Moho, only six 1D models could be used as constraints (stations TWC, ENA, EHC, TWD, HWA and CHK, Fig. S4 and Table S1). The mismatch ranges between 22 km and less than 1 km. Six out of seven constraints lie below the contoured surface (Fig. 9c). The two stations with the large mismatch (EHC and ENA) reveal rather low

Vp gradients at Moho depth, whereas the other four stations show stronger Vp gradients. This suggests that the same criteria apply as with the constraints for the Eurasian Moho above.

We also compared our interpolated Moho surfaces with Moho depths estimated from receiver functions using the P-to-S converted phase (Wang et al., 2010). For most parts of the eastwards subducting

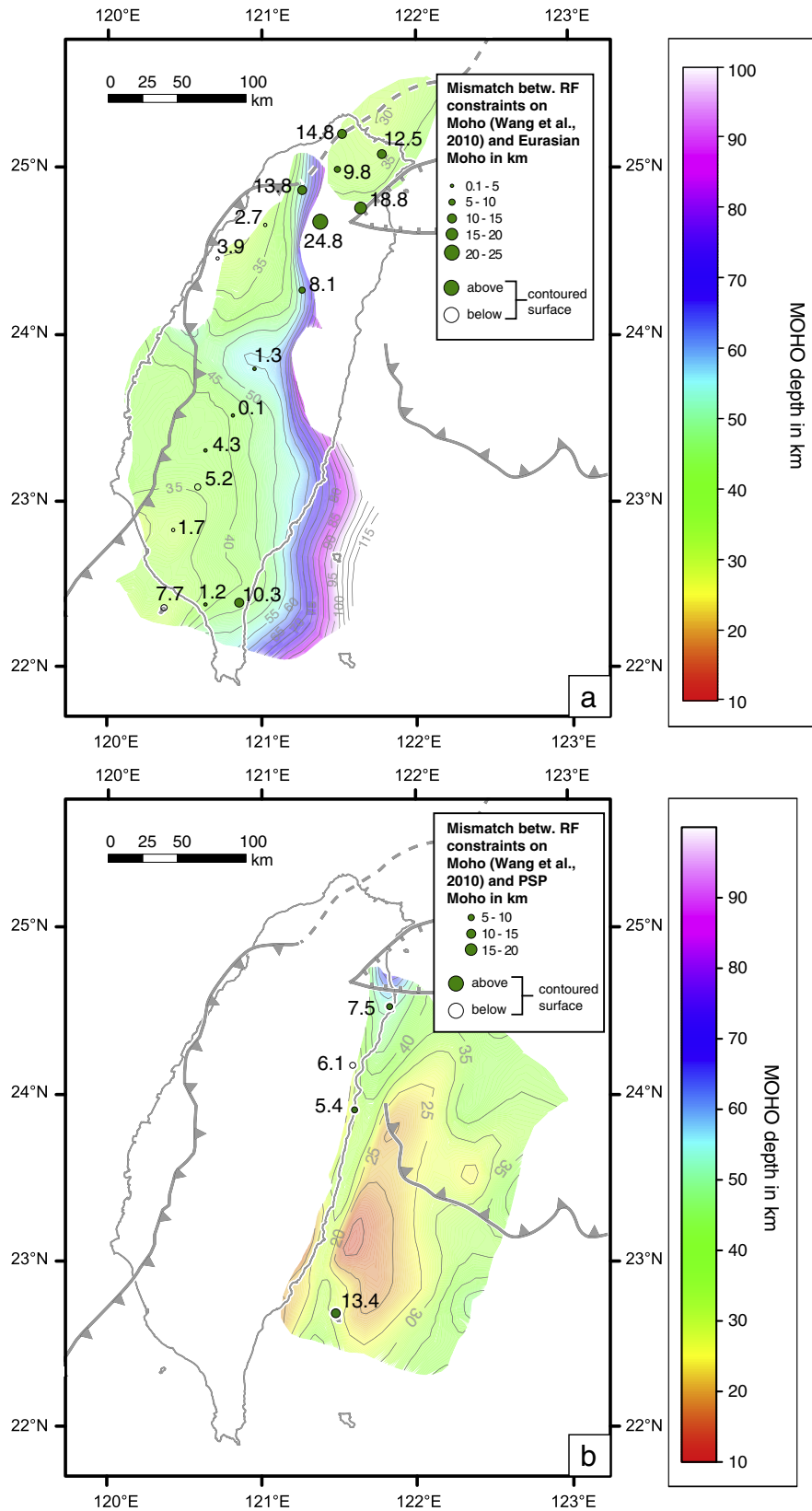


Fig. 10. (a) Map of the Eurasian Moho (same as Fig. 8a) and (b) the Philippine Sea plate Moho (same as Fig. 9a), showing the mismatch (i.e. vertical distance between the modeled surface and Moho depth constrained by receiver functions (Wang et al., 2010).

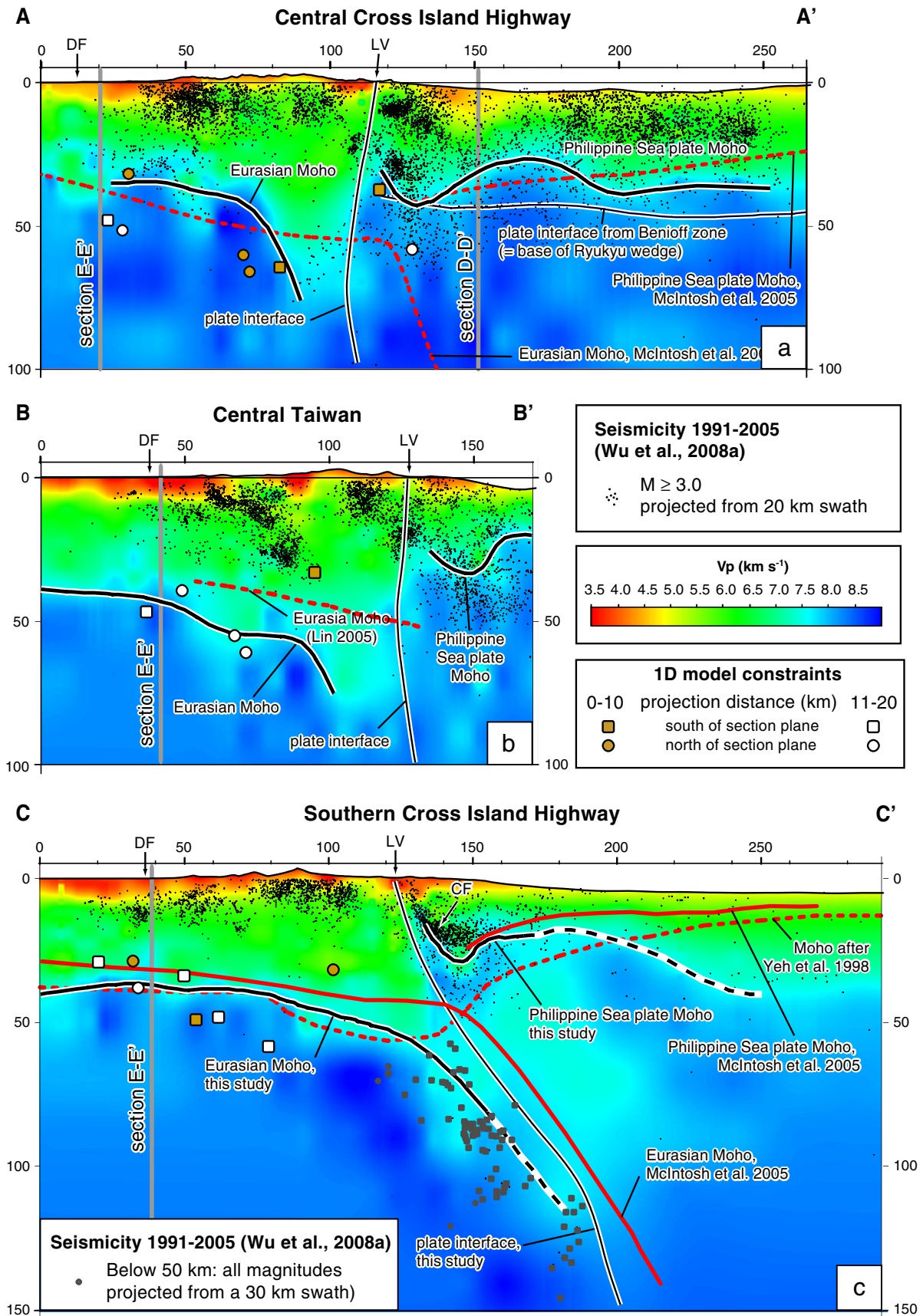


Fig. 11. Cross sectional views of plate interfaces and Moho surfaces derived in this study in comparison to previously published data. Sections A–A' to C–C' are parallel to various geophysical transects. Section E–E' (e) is parallel to a set of geological cross sections through the westernmost Foothills Thrust Belt (from Huang et al., 2004). (f) Location map of the sections. Scale is in kilometers. The Moho is dashed, where constrained by less than 500 (Eurasia) and 5000 (Philippine Sea plate) p-wave readings (compare Figs. 8b and 9b). 'CF' = Chihshang fault, 'DF' = deformation front, 'LV' = Longitudinal Valley.

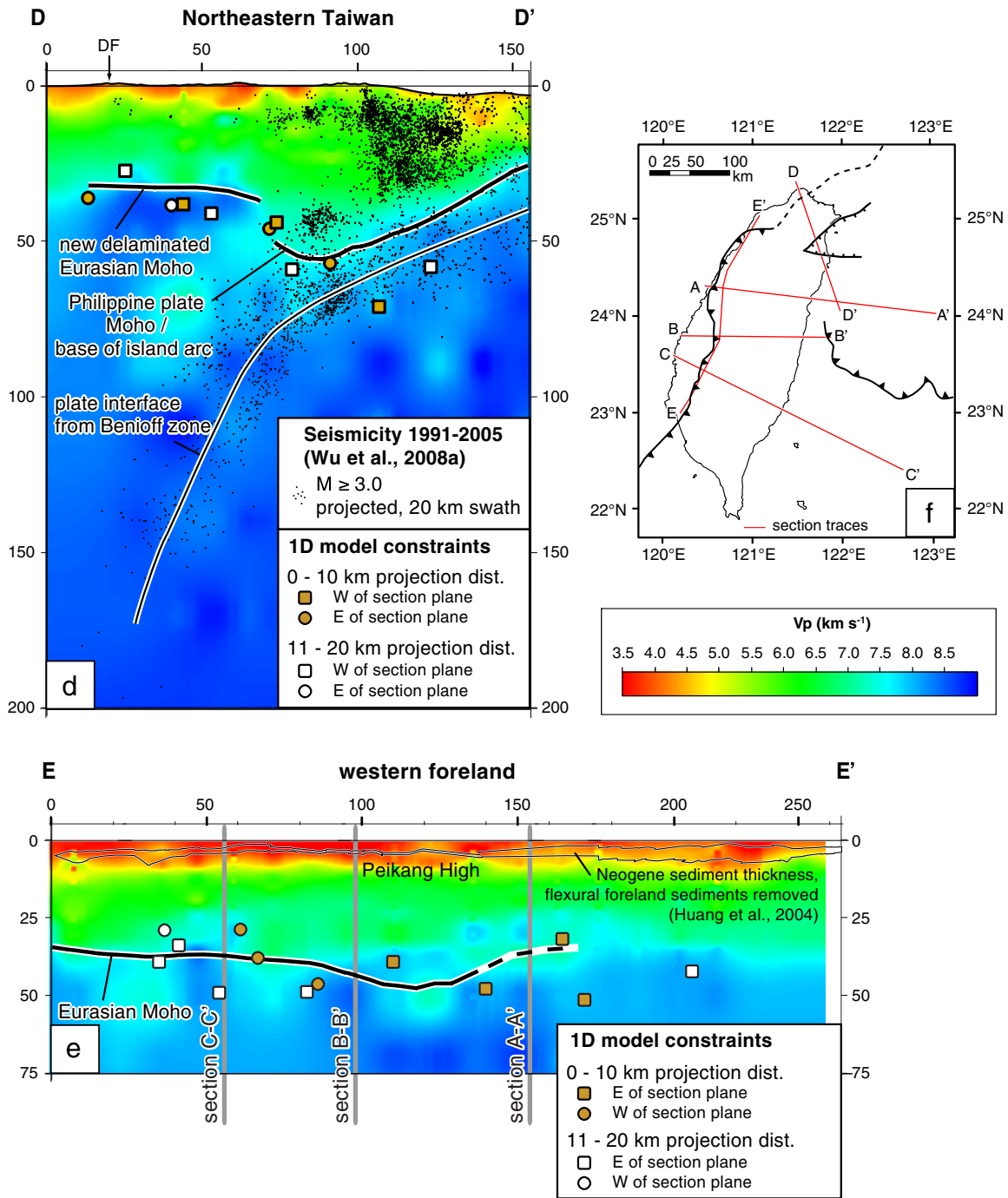


Fig. 11. (continued).

Moho, this mismatch is generally less than 10 km (Fig. 10a). The mismatch is much larger for the subhorizontal Moho identified underneath northeastern Taiwan. There, Wang et al. (2010) suggest a Moho depth between 17 and 24 km, about 5 to 10 km shallower than that constrained from tomography (Fig. 10a). Fig. 10b shows mismatch of the receiver function-derived Moho depth of Wang et al. (2010) with respect to the Philippine Sea plate Moho derived in this study.

4.2. Cross-sections across the Moho surfaces

The plate interface and Moho surfaces modeled in this study are shown in several cross sections together with the 1D model constraints, the seismicity distribution (Wu et al., 2008a), as well as results from previous studies (Fig. 11). Section A–A' (Fig. 11a) coincides with the wide-angle seismic profile Line 16 of McIntosh et al. (2005). Section B–B' (Fig. 11b) is parallel to a geophysical transect

provided by Lin (2005), extending further to the west and east. Section C–C' (Fig. 11c) coincides with yet another wide-angle seismic profile (McIntosh et al., 2005; Yeh et al., 1998). In Section C–C' we notice good agreement between the Eurasian Moho derived in this study with that of Yeh et al. (1998) under the western foreland and the Central Range. East of the Longitudinal Valley, the Eurasian Moho mapped in our study continues to dip further to the east, whereas that of Yeh et al. (1998) rises towards the Philippine Sea. The Eurasian and Philippine Sea Mohos derived by McIntosh et al. (2005) are roughly compatible with our results. However, the east-dipping part of the Eurasian Moho of McIntosh et al. (2005) is slightly more to the east. We give preference to our model of the Eurasian Moho and the plate interface, because they better correlate with the location of subduction-related earthquake hypocenters below a depth of 50 km, projected onto the section from a 30 km wide swath (Fig. 11c). The east-dipping part of the Philippine Sea plate Moho in Section C–C', immediately east of the plate interface, is well constrained by a pronounced Vp contrast. In addition, it is delineated by a plane of seismicity known as the Chihshang or Chengkung fault (Ching et al., 2007; Kim et al., 2006; Kuo Chen et al., 2007; Lee et al., 2006). Possibly, this plane of seismicity ('CF' in Fig. 11c) marks a lithosphere-scale fault delimiting a sliver of fore-arc lithosphere, which subducts underneath the island arc (Boutelier et al., 2003; Chemenda et al., 1997, 2001), towards east. At greater depth, we furthermore notice anomalous p-wave velocities as low as 7.6 km s^{-1} within the upper plate mantle lithosphere, overlying the plate interface between c. 30 and 80 km depth (Fig. 11c). Owing to this anomaly, the Vp gradient across the plate interface in this transect is low compared to, e.g., Sections A–A' and B–B'. This subjects the position of the plate interface to some uncertainty if judged from Vp alone. However, the fact that the plate interface aligns with the Benioff zone earthquakes (Fig. 11c, see above) makes our interpretation seem viable. It is conceivable that the described low Vp anomaly represents a partly serpentinized fore-arc mantle wedge (cf. Hyndman and Peacock, 2003, and references therein), which is being subducted underneath the island arc. However, it was beyond the scope of our study to explore this any further.

Comparing Sections A–A' to C–C' (Fig. 11a–c), we make the following major observations: (1) The Eurasian Moho steepens from 50° dip in Section C–C' to 70° dip in Section A–A'. (2) Similarly, the plate interface also steepens into vertical (and locally overturns) towards north. (3) The east-dipping portion of the Eurasian Moho and the plate interface (which together form the subducting Eurasian slab) step back towards the west, i.e., into a more external position with respect to the thrust belt structures exposed at surface. This becomes clearer when we consider the Longitudinal Valley and the deformation front as reference points in all three sections ('LV' and 'DF' in Fig. 11a–c, respectively). Between Sections A–A' and C–C', all surface geological units trend c. NNE–SSW and are mutually parallel (Fig. 1b). By contrast, the Eurasian Moho trends N–S from 23.5°N northwards (Fig. 8). This means that the thrust belt orientation departs increasingly from that of the hinge of the subducting Eurasian slab (compare Figs. 1b and 8). This suggests a progressive rollback and decoupling of the subducting slab from its original crust and lithosphere. The rollback hence assists in the polarity reversal in that it creates the space required for the Philippine Sea slab to subduct northwards underneath the Eurasian plate. Section D–D' (Fig. 11d) is located where the subduction polarity is already reversed. Here, the magmatic crustal root, interpreted as the base of the Philippine Sea plate Moho, overlies the Benioff zone, suggesting that the island arc was accreted to the base of the Ryukyu wedge on the upper plate rather than to become subducted with the rest of the Philippine Sea plate. Such accretion requires decoupling of the island arc crust from the rest of the subducting Philippine Sea plate, which could possibly be favored by lower bulk densities of intermediate to felsic arc material in comparison with oceanic crust. Accretion could have

occurred either during initial collision, while Eurasia subducted underneath the arc, or later when the arc began subducting underneath the Ryukyu trench.

Section E–E' (Fig. 11e) runs along-strike the Western Foothills thrust belt in close proximity to the deformation front and parallels a series of geological sections constrained by surface and subsurface data (Sections N1 to N4 in Huang et al., 2004) and will be discussed in the following.

4.3. Travel time residuals

The travel time residuals obtained from the 1D models (Fig. 6) generally increase eastward. They either represent (a) actual lateral velocity variations along the Moho discontinuity, or (b) indicate where the crustal structure departs from a simple horizontally layered crust as specified by the initial velocity model. We have no arguments to support or disregard lateral velocity variations at the Moho. Independent of that, evidence presented in Sections 2 and 3 suggests that the Eurasian Moho significantly departs from a simple horizontal structure, dipping eastwards underneath the Philippine Sea plate (Figs. 8, 9 and 11), i.e., where the largest residuals occur. By contrast, the crust can be inferred to represent a fairly horizontally layered structure where residuals are low, i.e., under western and southwestern Taiwan. The minimal travel time residuals of about 0.05 sec in central Taiwan define a circular area of c. $50 \times 70 \text{ km}$. Interestingly, this area roughly coincides with the Peikang High (e.g., Cheng et al., 2003; Huang et al., 2004; Lin and Watts, 2003; Mouthereau et al., 2002; Yang et al., 2006), a foreland area marked by a slight recess of the thrust belt front and reduced subsidence during the Neogene compared with northerly and southerly adjacent areas (see along strike Section E–E', Fig. 11e). The near-surface parts of Section E–E' show the thickness of the Neogene sediments up to the top of the Chinshui Shale, that is, disregarding the sediments related to flexural foreland subsidence since about 2.6 Ma (Chen et al., 2001). Stratigraphic successions repeated along thrust faults have been removed. The sediment interval depicted by the black outlines (Fig. 11e) thus represents the sediments deposited on the passive margin of the South China Sea before the onset of arc-continent collision. Discrete along-strike thickness changes of this sediment layer are due to faults, which were omitted for reasons of legibility. There is a slightly deeper Eurasian Moho, where the Neogene pre-collisional sediment thickness is reduced, i.e., on the Peikang High. It seems reasonable to assume that there is a relation between a deeper Moho and reduced Neogene sedimentation (and vice versa) in conjunction with the formation of the South China Sea passive margin, which was accompanied by lithospheric thinning through normal faulting (e.g., Ho, 1988; Lin and Watts, 2003; Teng and Lin, 2004). Following this line of reasoning, the Peikang High, unaffected by lithospheric thinning, likely retained its original crustal thickness. Lithospheric extension during passive margin formation possibly altered the velocity structure of the Eurasian crust underneath the foreland. In turn, this means that the crustal structure underlying the Peikang High possibly matches the input velocity model (Chen and Shin, 1988) best.

4.4. Crustal thickness in the western Philippine Sea plate

A velocity model along-strike the Ryukyu accretionary wedge (McIntosh and Nakamura, 1998), north of the Ryukyu trench, reported a crustal thickness of c. 30 km. This is in agreement with our results, which possibly also suggest the basal accretion of island arc crust and, correspondingly, crustal thickening (Fig. 11e). However, our tomography-derived isovelocity surface for the Philippine Sea plate Moho suggests a depth between 25 and 35 km also in the area south of the Ryukyu trench and east of the Luzon arc (Fig. 9). Given that crustal thickening of the oceanic crust by accretion is not expected there, this value is anomalously high. Deschamps et al. (2000) reported Early Cretaceous $^{40}\text{Ar}/^{39}\text{Ar}$ ages on dredged gabbros

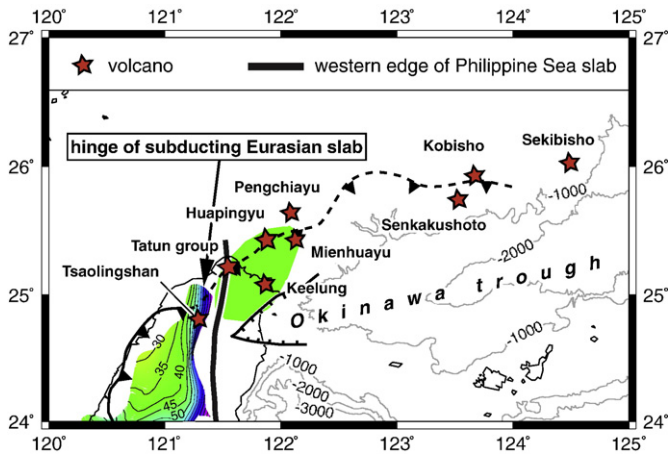


Fig. 12. Position of the post-collisional North Taiwan volcanic province (after Wang et al., 1999; 2004) in relation to the deformation front and some crust–mantle boundaries derived in this study. The volcanoes terminate at the western confinement of the north-dipping Philippine Sea slab and are underlain by a subhorizontal Moho. The transition from the active to the inactive segment of the deformation front (after Hsiao et al., 1998) coincides with the hinge of the subducting Eurasian slab at the level of the Moho. In combination, this suggests a progressive deactivation of the deformation by the westward encroachment of the Philippine Sea slab.

from the Western Philippine Sea between 115 and 125 Ma. These authors also noticed that the basin, with an average water depth around 5000 m, is about 400 m shallower than theoretically expected for oceanic basement of such age. Shallower water depth is expected if the crust is anomalously thick, making the lithosphere more buoyant. Such an interpretation is in conflict with results of McIntosh et al. (2005), who, based on a wide-angle seismic survey (their Line 23), reported a thickness of the Philippine Sea plate of merely 10 to 15 km east of the Luzon arc. The discrepancy between their model and our tomography-derived Moho depth is particularly clear in Section C–C' (Fig. 11c). We presume that the geometry of the Philippine Sea plate Moho east of Taiwan is less well constrained by the tomography due to much sparser station distribution and low number of Vp readings per tomographic cell. Possibly, also the input velocity model (Chen and Shin, 1988), optimized for the crust and lithosphere underneath mainland Taiwan, is partly inadequate. Hence, we consider the geometry of the tomography-derived Philippine Sea plate Moho in regions constrained by less than 5000 Vp readings (Fig. 9b) as poorly constrained.

4.5. Indications for progressive subduction polarity flip along the Eurasian margin

We noticed that the eastward subducting Eurasian slab (imaged by the Eurasian Moho and the plate interface) rolls back towards the autochthonous foreland in more northerly transects (Fig. 11). Here, we further explore the implications arising from this. The Eurasian slab is essentially vertical and trends c. N–S from about 24°N northwards (Fig. 12). North of 25°N, the hinge of the slab intersects the deformation front, implying its rollback towards the autochthonous foreland. The position of the hinge coincides with the transition from an active to inactive thrust front (Hsiao et al., 1998; Figs. 8 and 12). East of the subducting Eurasian slab, i.e. along the inactive segment of the thrust front, a subhorizontal Eurasian plate Moho was mapped, overlying the north-dipping Philippine Sea slab (Figs. 7a,b,

8a and 12). The inactive parts of the thrust front coincide with a NE–SW-trending chain of volcanic islets and a few onshore volcanoes, referred to as North Taiwan Volcanic Province (Wang et al., 1999; Fig. 12). Magmatic activity within this province is post-collisional, commencing at 2.8–2.5 Ma and lasting into the Quaternary (Wang et al., 1999; 2004). A progression of volcanic activity from northeast to southwest was suggested (Teng et al., 1992; Teng, 1996), but questioned more recently (Wang et al., 2004). Independent of this, the magmas show systematic compositional variations from low-K over calc-alkaline to shoshonitic affinities from NE to SW. This was explained by variable degrees of partial melting of an ascending asthenospheric mantle (Wang et al., 2004), triggered by post-collisional, extensional collapse of the northern Taiwan mountain belt (Teng, 1996), and interaction with the overlying, metasomatized lithospheric mantle. For some magmas (Mienhuayu island, Fig. 12), Wang et al. (2004) argued that asthenospheric upwelling was as shallow as 60 km, implying an abnormally thin lithosphere. More importantly still, the Mienhuayu lavas are not depleted in high field strength elements, suggesting magma generation in an intraplate rather than a subduction setting (Wang et al., 2004). In this context, the subhorizontal Moho identified underneath the inactive thrust front in northeastern Taiwan (Figs. 8a and 11d) possibly represents a new, subcontinental Moho that formed after substantial lithospheric thinning and/or asthenosphere upwelling. Conceivably, the original Eurasian lithosphere underneath northeastern Taiwan was thinned or removed by rollback and delamination, leaving the thrust front to the east inactive (Fig. 12) and triggering non-subduction related magmatism within the North Taiwan Volcanic Province.

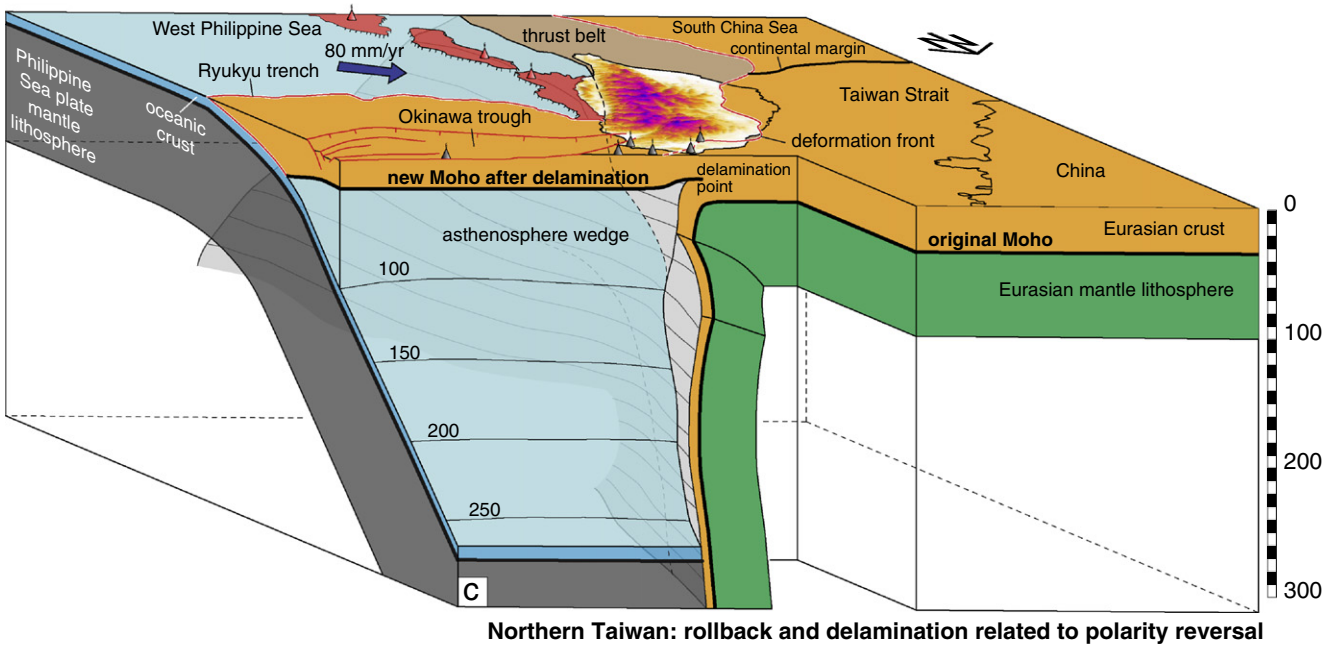
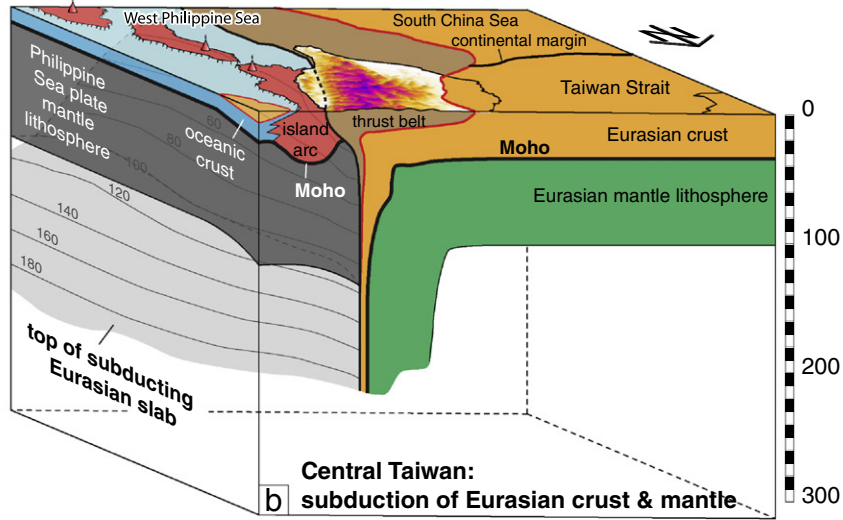
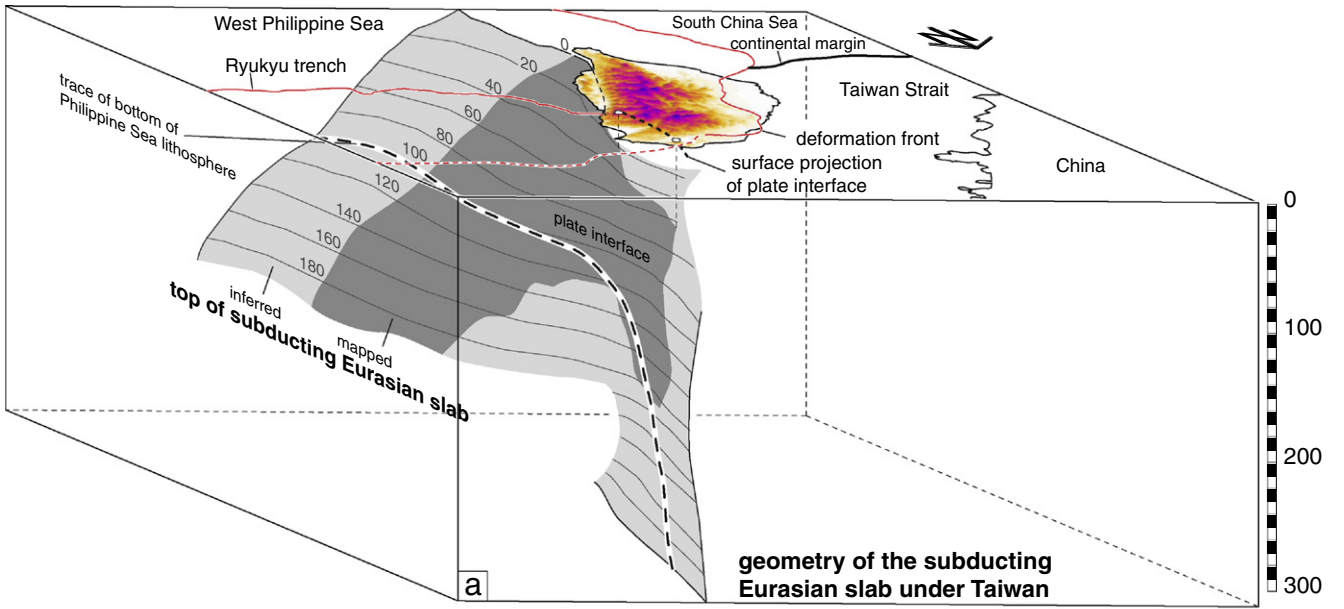
In summary, our structural model reveals a gradual steepening of the subducting Eurasian slab along-strike the mountain belt towards north (Fig. 13a). Rollback was possibly facilitated once the subducting Eurasian slab had steepened into vertical (Section A–A', Figs. 11a and 13b). Underneath northernmost Taiwan, rollback and delamination of the Eurasian slab have advanced into the foreland, leaving the thrust front east of the hinge of the subducting slab inactive. In addition, delamination has triggered the post-collisional magmatism by leaving a shallow asthenosphere wedge behind the delamination front (Fig. 13c). The northward steepening of the subducting Eurasian slab and its subsequent rollback and delamination towards west provide the space that is required for the Philippine Sea plate to subduct northwards underneath Eurasia (Fig. 13a–c). Westward rollback of the delaminating Eurasian lithosphere, deactivation of compressional thrust belt structures and the migrating front of post-collisional magmatism in the North Taiwan Volcanic Province therefore all appear interrelated with the northward subduction of the Philippine Sea plate. We think that, in combination, these observations support a model of progressive subduction polarity flip, achieved by migrating a tear in the Eurasian lithosphere along the edge of the passive margin (Clift et al., 2003; Suppe, 1984; Fig. 2b).

5. Conclusions

Based on local earthquake tomography, 1D models and seismicity distribution, several important crust–mantle boundaries were mapped in the Taiwan–Luzon arc-continent collision zone.

- (1) The eastern limit of the Eurasian lower crust against the lithospheric mantle of the Philippine Sea plate represents the plate boundary interface. This interface dips steeply to the east underneath southeastern Taiwan. It steepens progressively

Fig. 13. Schematic lithosphere-scale block diagrams illustrating along-strike changes in the geometry of various crust–mantle boundaries under Taiwan, mapped in this study. The margins of the block domains trend N–S and E–W, respectively. Depth is given in km. (a) Geometry of the plate interface separating the Eurasian and Philippine Sea plates. The plate interface progressively steepens from south to north. (b) Section through central Taiwan at c. 24°N, where the subducting Eurasian slab is vertical. A thickness of 100 km is assumed for both the Eurasian and Philippine Sea plates. (c) Section at the northern tip of Taiwan, illustrating the rollback and delamination of the subducting Eurasian lithosphere. This creates the space required for the Philippine Sea plate to subduct northward. The deactivation of the deformation front occurs at the hinge of the subducting and delaminating Eurasian lithosphere. The shallow asthenosphere wedge east of the delamination front provides the source for the north Taiwan volcanoes (in gray).



towards north and becomes vertical at 23.7°N. From there it continues northward in a vertical orientation, until the limit of the tomographic model at the northern tip of Taiwan inhibited further mapping. Towards east, the plate interface abuts the north-dipping Benioff zone of the Philippine Sea slab. Topologically, these two planes define the bottom and top of the Philippine Sea plate, respectively.

- (2) The tomographically defined Eurasian Moho dips to the E at 50–60° in southeastern Taiwan, following the trend of the plate boundary. Towards the north, this Moho steepens into subvertical, again mimicking the orientation of the plate boundary. At the same time, it steps westward into a more external position underneath the thrust belt, giving way to the north-dipping Philippine Sea plate. Parts of northeastern Taiwan hence lack their Eurasian lower crustal and lithospheric underpinning, but are underlain by the Philippine Sea plate.
- (3) The tomographically defined Moho of the Philippine Sea plate is substantially shallower than the Eurasian Moho across much of Central Taiwan, and in an upper plate position south of the Ryukyu trench. It shallows towards the surface along the Longitudinal Valley suture and exhibits a crustal root parallel to the trend of surface geological units. The root is interpreted as the deformed Luzon arc and fore-arc. Towards north, the Luzon arc/fore-arc root progressively deepens from 30 to about 70 km depth underneath the Ryukyu trench. The base of the crustal root lies above the Benioff zone, suggesting its possible accretion to the base of the overlying Eurasian upper plate.
- (4) Underneath northernmost Taiwan, the subducting Eurasian slab has advanced into the foreland by rollback and delamination, leaving the thrust front behind the hinge of the subducting slab inactive. A subhorizontal Moho at 30–35 km depth formed behind the delamination front and overlies the north-dipping Philippine Sea slab. In addition, rollback and delamination have triggered post-collisional magmatism by leaving a shallow asthenosphere wedge behind the delamination front. In combination, these data support a model of a progressive subduction polarity flip by progressing a tear in the Eurasian lithosphere along the former edge of the passive margin.

Supplementary materials related to this article can be found online at doi:10.1016/j.tecto.2011.12.029.

Acknowledgments

We thank Lionel Sime for the editorial handling of our contribution. The manuscript benefitted from very thorough reviews by two anonymous colleagues, as well as from additional helpful comments by Dennis Brown, David Boutelier, Kirk McIntosh, Jean-Philippe Avouac and Mark Handy. K.U. appreciates financial support through project NSC 97-2811-M-002-082 of the National Science Council of Taiwan. Several figures were made using GMT, the General Mapping Tool (Wessel and Smith, 1998).

References

- Angelier, J., 1986. Geodynamics of the Eurasia-Philippine Sea Plate boundary: preface. *Tectonophysics* 125, 9–10.
- Boutelier, D., Chemenda, A.I., Burg, J.-P., 2003. Subduction versus accretion of intra-arc volcanic arcs: insight from thermo-mechanical analogue experiments. *Earth and Planetary Science Letters* 212, 31–45.
- Brown, D., Llana-Funez, S., Carbonell, R., Alvarez-Marron, J., Marti, D., Salisbury, M., 2009. Laboratory measurements of P-wave and S-wave velocities across a surface analog of the continental crust–mantle boundary: Cabo Ortegal, Spain. *Earth and Planetary Science Letters* 285, 27–38.
- Burtman, V.S., Molnar, P., 1993. Geological and geophysical evidence for deep subduction of continental crust beneath the Pamir. *Special Papers*, 281. Geological Society of America. 1–76 pp.
- Chang, S.S.L., Chi, W.-R., 1983. Neogene nannoplankton biostratigraphy in Taiwan and the tectonic implications. *Petroleum Geology of Taiwan* 19, 93–147.
- Chemenda, A.I., Yang, R.K., Hsieh, C.H., Groholsky, A.L., 1997. Evolutionary model for the Taiwan collision based on physical modelling. *Tectonophysics* 274, 253–274.
- Chemenda, A.I., Yang, R.-K., Stephan, J.-F., Konstantinovskaia, E.A., Ivanov, G.M., 2001. New results from physical modelling of arc-continent collision in Taiwan: evolutionary model. *Tectonophysics* 333, 159–178.
- Chen, Y.-L., Shin, T.-C., 1988. Study on the earthquake location of 3-D velocity structure in the Taiwan area. *Meteorological Bulletin* 42, 135–169.
- Chen, W.-S., Ridgway, K.D., Horng, C.-S., Chen, Y.-G., Shea, K.-S., Yeh, M.-G., 2001. Stratigraphic architecture, magnetostratigraphy, and incised-valley systems of the Pliocene–Pleistocene collisional marine foreland basin of Taiwan. *GSA Bulletin* 113, 1249–1271.
- Chen, C.H., Chen, Y.H., Yen, H.Y., Yu, G.K., 2003. Lateral variations of Pn velocity and anisotropy in Taiwan from travel-time tomography. *Earth Planets Space* 55, 223–230.
- Chen, P.-F., Huang, B.-S., Liang, W.-T., 2004. Evidence of a slab of subducted lithosphere beneath central Taiwan from seismic waveforms and travel times. *Earth and Planetary Science Letters* 229, 61–71.
- Cheng, W.-B., 2009. Tomographic imaging of the convergent zone in Eastern Taiwan – a subducting forearc sliver revealed? *Tectonophysics* 466, 170–183.
- Cheng, W.-B., Huang, H.-C., Wang, C., Wu, M.-S., Hsuan, T.-H., 2003. Velocity structure, seismicity and fault structure in the Peikang High area of western Taiwan. *Terrestrial, Atmospheric and Oceanic Sciences* 14, 63–83.
- Chi, W.-R., Namson, J., Suppe, J., 1981. Stratigraphic record of plate interactions in the Coastal Range of Eastern Taiwan. *Memoir of the Geological Society of China* 4, 155–194.
- Ching, K.-E., Rau, R.-J., Zeng, Y., 2007. Coseismic source model of the 2003 Mw 6.8 Chengkung earthquake, Taiwan, determined from GPS measurements. *Journal of Geophysical Research* 112, B06422.
- Chou, H.-C., Kuo, B.-Y., Hung, S.-H., Chiao, L.-Y., Zhao, D., Wu, Y.-M., 2006. The Taiwan-Ryukyu subduction-collision complex: folding of a viscoelastic slab and the double seismic zone. *Journal of Geophysical Research* 111, B04410. doi:10.1029/2005JB003822.
- Christensen, N.I., Mooney, W.D., 1995. Seismic velocity structure and composition of the continental crust: a global view. *Journal of Geophysical Research* 100, 9761–9788.
- Clift, P.D., Schouten, H., Draut, A.E., 2003. A general model of arc-continent collision and subduction polarity reversal from Taiwan and the Irish Caledonides. *Geological Society of London. Special Publication* 219, 81–98.
- Deschamps, A., Monié, P., Lallemand, S., Hsu, S.K., Yeh, K.Y., 2000. Evidence for Early Cretaceous oceanic crust trapped in the Philippine Sea Plate. *Earth and Planetary Science Letters* 179, 503–516.
- Ernst, W.G., 1983. Mountain building and metamorphism: a case study from Taiwan. In: Hsu, K.J. (Ed.), *Mountain Building*. Academic Press, London, pp. 247–256.
- Giese, P., Scheuber, E., Schilling, F., Schmitz, M., Wigger, P., 1999. Crustal thickening processes in the Central Andes and the different natures of the Moho-discontinuity. *Journal of South American Earth Sciences* 12, 201–220.
- Goldberg, D.E., 1989. *Genetic Algorithms in Search, Optimization, and Machine Learning*. Addison-Wesley, Boston. 372 pp.
- Ho, C.S., 1988. *An Introduction to the Geology of Taiwan*. Explanatory text of the geologic map of Taiwan. Central Geological Survey. Ministry of Economic Affairs, Taiwan, Republic of China, Taipei. 192 pp.
- Holland, J.H., 1975. *Adaptation in Natural and Artificial Systems*. The University of Michigan Press, Ann Arbor.
- Hsiao, L.-Y., Lin, K.-A., Huang, S.-T., Teng, L.S., 1998. Structural characteristics of the Southern Taiwan-Sinzi folded zone. *Petroleum Geology of Taiwan* 32, 133–153.
- Hsu, H.-J., Wen, S., Chen, C.-H., 2011. 3D topography of the Moho discontinuity in the Taiwan area as extracted from travel time inversion of PmP phases. *Journal of Asian Earth Sciences* 41, 335–343.
- Huang, S.-T., Yang, K.-M., Ting, H.-H., Lee, C.-J., 2004. Observation of fault activity and evaluation of the earthquake potential in the Western foothills area of Taiwan, based on the synthetic analysis of subsurface data (in Traditional Chinese). Report to the Central Geological Survey Taiwan. 71 pp.
- Hyndman, R.D., Peacock, S.M., 2003. Serpentinization of the forearc mantle. *Earth and Planetary Science Letters* 212, 417–432.
- Jarchow, C.M., Thompson, G.A., 1989. The nature of the Mohorovičić discontinuity. *Annual Review of Earth and Planetary Sciences* 17, 475–506.
- Kao, H., Rau, R.-J., 1999. Detailed structures of the subducted Philippine Sea plate beneath northeast Taiwan: a new type of double seismic zone. *Journal of Geophysical Research* 104, 1015–1033.
- Kao, H., Huang, G.-C., Liu, C.-S., 2000. Transition from oblique subduction to collision in the northern Luzon arc-Taiwan region: constraints from bathymetry and seismic observations. *Journal of Geophysical Research* 105, 3059–3079.
- Kim, K.H., Chiu, J.M., Kao, H., Liu, Q., Yeh, Y.-H., 2004. A preliminary study of crustal structure in Taiwan region using receiver function analysis. *Geophysical Journal International* 159, 146–164.
- Kim, K.-H., Chiu, J.-M., Pujol, J., Chen, K.-C., Huang, B.-S., Yeh, Y.-H., Shen, P., 2005. Three-dimensional V_p and V_s structural models associated with the active subduction and collision tectonics in the Taiwan region. *Geophysical Journal International* 162, 204–220.
- Kim, K.H., Chiu, J.M., Pujol, J., Chen, K.C., 2006. Polarity reversal of active plate boundary and elevated oceanic upper mantle beneath the collision suture in Central Eastern Taiwan. *Bulletin of the Seismological Society of America* 96, 796–806.
- Kissling, E., Schmid, S.M., Lippitsch, R., Ansorge, J., Fügenschuh, B., 2006. Lithosphere structure and tectonic evolution of the Alpine arc: new evidence from high-

- resolution teleseismic tomography. In: Gee, D.G., Stephenson, R.A. (Eds.), *European Lithosphere Dynamics*. Geological Society London Memoirs, London, pp. 129–145.
- Kuoehen, H., Wu, Y.-M., Chen, Y.-G., Chen, R.-Y., 2007. 2003 Mw6.8 Chengkung earthquake and its related seismogenic structures. *Journal of Asian Earth Sciences* 31, 332–339.
- Lallemand, S., Font, Y., Bijwaard, H., Kao, H., 2001. New insights on 3-D plates interaction near Taiwan from tomography and tectonic implications. *Tectonophysics* 335, 229–253.
- Lee, W.H.K., Lahr, J.C., 1975. HYP071 (Revised): A Computer Program for Determining Hypocenter, Magnitude and First Motion Pattern of Local Earthquakes, U.S. Geological Survey Open-file Report 75–311, p. 114.
- Lee, J.-C., Chu, H.-T., Angelier, J., Hu, J.-C., Chen, H.-Y., Yu, S.-B., 2006. Quantitative analysis of surface coseismic faulting and postseismic creep accompanying the 2003, Mw = 6.5, Chengkung earthquake in eastern Taiwan. *Journal of Geophysical Research* 111, B02405.
- Letouzey, J., Kimura, M., 1986. The Okinawa Trough: genesis of a back-arc basin developing along a continental margin. *Tectonophysics* 125, 209–230.
- Li, C., van der Hilst, R.D., Engdahl, E.R., Burdick, S., 2008. A new global model for P wave speed variations in Earth's mantle. *Geochemistry, Geophysics, Geosystems* 9, Q05018.
- Liang, W.-T., Chiu, J.-M., Kim, K., 2007. Anomalous Pn waves observed in Eastern Taiwan: implications of a thin crust and elevated oceanic upper mantle beneath the active collision-zone suture. *Bulletin of the Seismological Society of America* 97, 1370–1377.
- Lin, C.-H., 2000. Thermal modeling of continental subduction and exhumation constrained by heat flow and seismicity in Taiwan. *Tectonophysics* 324, 189–201.
- Lin, C.-H., 2002. Active continental subduction and crustal exhumation: the Taiwan orogeny. *Terra Nova* 14, 281–287.
- Lin, C.-H., 2005. Identification of mantle reflections from a dense linear seismic array: tectonic implications to the Taiwan orogeny. *Geophysical Research Letters* 32, L06315.
- Lin, C.-H., 2009. Compelling evidence of an aseismic slab beneath central Taiwan from a dense linear seismic array. *Tectonophysics* 466, 205–212.
- Lin, C.-H., Roecker, S.W., 1993. Deep earthquakes beneath central Taiwan: mantle shearing in an arc-continent collision. *Tectonics* 12, 745–755.
- Lin, A.T., Watts, A.B., 2003. Cenozoic stratigraphy and subsidence history of the South China Sea margin in the Taiwan region. *Basin Research* 15, 453–478. doi:10.1046/j.1365-2117.2003.00215.x.
- Lippitsch, R., Kissling, E., Ansgor, J., 2003. Upper mantle structure beneath the Alpine orogen from high-resolution teleseismic tomography. *Journal of Geophysical Research* 108 (B8), 2376. doi:10.1029/2002JB002016.
- Ma, K.-F., Liu, N.-J., 1997. The images of subduction slabs in the Taiwan region. *Journal of the Geological Society of China* 40, 653–670.
- Ma, K.-F., Song, D.-R., 1997. Pn velocity and MOHO depth in Taiwan. *Journal of the Geological Society of China* 40, 167–184.
- Ma, K.-F., Song, T.-R.A., 2004. Thermo-mechanical structure beneath the young orogenic belt of Taiwan. *Tectonophysics* 388, 21–31.
- Ma, K.-F., Wang, J.-H., Zhao, D., 1996. Three-dimensional seismic velocity structure of the crust and uppermost mantle beneath Taiwan. *Journal of the Physics of the Earth* 44, 85–105.
- Malavieille, J., Lallemand, S.E., Dominguez, S., Deschamps, A., Lu, C.-Y., Liu, C.-S., Schnuerle, P., Angelier, J., Collot, J.Y., Deffontaines, B., Fournier, M., Hsu, S.K., Le Formal, J.P., Liu, S.Y., Sibuet, J.C., Thareau, N., Wang, F., ACT (Active Collision in Taiwan) Scientific Crew, 2002. Arc-continent collision in Taiwan: new marine observations and tectonic evolution. *Geological Society of America Special Paper* 358, 187–211.
- Mallet, J.L., 1992. Discrete smooth interpolation in geometric modelling. *Computer-Aided Design* 24, 178–191.
- McIntosh, K.D., Nakamura, Y., 1998. Crustal structure beneath the Nanao forearc basin from TAICRUST MCS/OBS line 14. *Terrestrial, Atmospheric and Oceanic Sciences* 9, 345–362.
- McIntosh, K., Nakamura, Y., Wang, T.-K., Shih, R.-C., Chen, A., Liu, C.-S., 2005. Crustal-scale seismic profiles across Taiwan and the western Philippine Sea. *Tectonophysics* 401, 23–54.
- McKenzie, D.P., Morgan, W.J., 1969. Evolution of triple junctions. *Nature* 224, 125–133.
- Molli, G., Malavieille, J., 2011. Orogenic processes and the Corsica/Apennines geodynamic evolution: insights from Taiwan. *International Journal of Earth Sciences* 100, 1207–1224.
- Mooney, W.D., 2007. Crust and lithospheric structure – global crustal structure. In: Romanowicz, B., Dziewonski, A. (Eds.), *Treatise on Geophysics, Volume 1: Seismology and the Structure of the Earth*. Elsevier, pp. 361–417.
- Mouthereau, F., Deffontaines, B., Lacombe, O., Angelier, J., 2002. Variations along the strike of the Taiwan thrust belt: basement control on structural style, wedge geometry, and kinematics. *Geological Society of America Special Paper* 358, 31–54.
- Pegler, G., Das, S., 1998. An enhanced image of the Pamir–Hindu Kush seismic zone from relocated earthquake hypocenters. *Geophysical Journal International* 134, 573–595.
- Press, F., 1966. Seismic velocities. In: Clark, S.P. (Ed.), *Handbook of Physical Constants*. Geological Society of America Memoir. Geological Society of America, pp. 196–218.
- Rau, R.-J., Wu, F.T., 1995. Tomographic imaging of lithospheric structures under Taiwan. *Earth and Planetary Science Letters* 133, 517–532.
- Reed, D.L., Lundberg, N., Liu, C.H., Kuo, B.-Y., 1992. Structural relations along the margins of the offshore Taiwan accretionary wedge: implications for accretion and crustal kinematics. *Acta Geologica Taiwanica* 30, 105–122.
- Roecker, S.W., Yeh, Y.-H., Tsai, Y.-B., 1987. Three-dimensional P and S wave velocity structures beneath Taiwan: deep structure beneath an arc-continent collision. *Journal of Geophysical Research* 92, 10,547–10,570.
- Seno, T., 1977. The instantaneous rotation vector of the Philippine Sea plate relative to the Eurasian plate. *Tectonophysics* 42, 209–226.
- Sibuet, J.-C., Hsu, S.-K., 2004. How was Taiwan created? *Tectonophysics* 379, 159–181.
- Sibuet, J.-C., Hsu, S.-K., Le Pichon, X., Le Formal, J.-P., Reed, D., Moore, G., Liu, C.-S., 2002. East Asia plate tectonics since 15 Ma: constraints from the Taiwan region. *Tectonophysics* 344, 103–134.
- Stein, S., Wysession, M., 2003. *An Introduction to Seismology, Earthquakes and Earth Structure*. Blackwell, 498 pp.
- Suppe, J., 1984. Kinematics of arc-continent collision, flipping of subduction, and back-arc spreading near Taiwan. *Memoir of the Geological Society of China* 6, 21–33.
- Suppe, J., Liou, J.G., Ernst, W.G., 1981. Paleogeographic origins of the Miocene East Taiwan Ophiolite. *American Journal of Science* 281, 228–246.
- Taylor, B., Hayes, D.E., 1983. Origin and history of the South China Sea Basin. *American Geophysical Union Monograph* 27, 23–56.
- Teng, L.S., 1990. Geotectonic evolution of late Cenozoic arc-continent collision in Taiwan. *Tectonophysics* 183, 57–76.
- Teng, L.S., 1996. Extensional collapse of the northern Taiwan mountain belt. *Geology* 24, 949–952.
- Teng, L.S., Lin, A.T., 2004. Cenozoic tectonics of the China continental margin: insights from Taiwan. *Geological Society of London. Special Publication* 226, 313–332.
- Teng, L.S., Chen, C.H., Wang, W.S., Liu, T.K., Juang, W.-S., Chen, J.-C., 1992. Plate kinematic model for late Cenozoic arc magmatism in northern Taiwan. *Journal of the Geological Society of China* 35, 1–18.
- Teng, L.S., Lee, C.T., Tsai, Y.B., Hsiao, L.-Y., 2000. Slab breakoff as a mechanism for flipping of subduction polarity in Taiwan. *Geology* 28, 155–158.
- Teng, L.S., Lee, C.T., Peng, C.H., Chen, W.F., Chu, C.J., 2001. Origin and geological evolution of the Taipei Basin, Northern Taiwan. *Western Pacific Earth Sciences* 1–2, 115–142.
- Tsai, Y.-B., 1986. Seismotectonics of Taiwan. *Tectonophysics* 125, 17–37.
- Tsai, Y.-B., Ten, T.L., Chiu, J.M., Liu, H.L., 1977. Tectonic implications of the seismicity in the Taiwan region. *Memoir of the Geological Society of China* 2, 13–41.
- Wageman, J.M., Hilde, T.W.C., Emery, K.O., 1970. Structural framework of East China Sea and Yellow Sea. *AAPG Bulletin* 54, 1611–1643.
- Wang, K.-L., Chung, S.-L., Chen, C.-H., Shinjo, R., Yang, T.F., Chen, C.-H., 1999. Post-collisional magmatism around northern Taiwan and its relation with opening of the Okinawa Trough. *Tectonophysics* 308, 363–376.
- Wang, K.-L., Chung, S.-L., O'Reilly, S.Y., Sun, S.-S., Shinjo, R., Chen, C.-H., 2004. Geochemical constraints for the genesis of post-collisional magmatism and the geodynamic evolution of the Northern Taiwan Region. *Journal of Petrology* 45, 975–1011.
- Wang, Z., Zhao, D., Wang, J., Kao, H., 2006. Tomographic evidence for the Eurasian lithosphere subducting beneath south Taiwan. *Geophysical Research Letters* 33, L18306. doi:10.1029/2006GL027166.
- Wang, Z., Fukao, Y., Zhao, D., Kodaira, S., Mishra, O.P., Yamada, A., 2009. Structural heterogeneities in the crust and upper mantle beneath Taiwan. *Tectonophysics* 476, 460–477.
- Wang, H.-L., Zhu, L., Chen, H.-W., 2010. Moho depth variation in Taiwan from teleseismic receiver functions. *Journal of Asian Earth Sciences* 37, 286–291.
- Wessel, P., Smith, W.H.F., 1998. New, improved version of generic mapping tools released. *EOS, Transactions of the American Geophysical Union* 79, 579.
- Wu, F.T., Rau, R.-J., Salzberg, D., 1997. Taiwan orogeny: thin-skinned or lithospheric collision? *Tectonophysics* 274, 191–220.
- Wu, Y.-M., Chang, C.-H., Zhao, L., Shyu, J.B.H., Chen, Y.-G., Sieh, K., Avouac, J.-P., 2007. Seismic tomography of Taiwan: improved constraints from a dense network of strong motion stations. *Journal of Geophysical Research* 112, B08312. doi:10.1029/2007JB004983.
- Wu, Y.-M., Chang, C.-H., Zhao, L., Teng, T.-L., Nakamura, M., 2008a. A comprehensive relocation of earthquakes in Taiwan from 1991 to 2005. *Bulletin of the Seismological Society of America* 98, 1471–1481.
- Wu, Y.-M., Zhao, L., Chang, C.-H., Hsu, Y.-J., 2008b. Focal mechanism determination in Taiwan by genetic algorithm. *Bulletin of the Seismological Society of America* 98, 651–661.
- Wu, F.T., Liang, W.-T., Lee, J.-C., Benz, H., Villaseñor, A., 2009a. A model for the termination of the Ryukyu subduction zone against Taiwan: a junction of collision, subduction/separation, and subduction boundaries. *Journal of Geophysical Research* 114, B07404. doi:10.1029/2008JB005950.
- Wu, Y.-M., Zhao, L., Chang, C.-H., Hsiao, N.-C., Chen, Y.-G., Hsu, S.-K., 2009b. Relocation of the 2006 Pingtung Earthquake sequence and seismotectonics in Southern Taiwan. *Tectonophysics* 479, 19–27.
- Wu, Y.-M., Shyu, J.B.H., Chang, C.-H., Zhao, L., Nakamura, M., Hsu, S.-K., 2009c. Improved seismic tomography offshore northeastern Taiwan: implications for subduction and collision processes between Taiwan and the southernmost Ryukyu. *Geophysical Journal International* 178, 1042–1054.
- Yang, K.-M., Huang, S.-T., Wu, J.-C., Ting, H.-H., Mei, W.-W., 2006. Review and new insights on foreland tectonics in Western Taiwan. *International Geology Review* 48, 910–941.
- Yeh, Y.H., Shih, R.-C., Lin, C.-H., Liu, C.H., Yen, H.Y., Huang, B.-S., Liu, C.-S., Chen, P.Z., Huang, C.S., Wu, C.J., Wu, F.T., 1998. Onshore/offshore wide-angle deep seismic profiling in Taiwan. *Terrestrial, Atmospheric and Oceanic Sciences* 9, 301–316.
- Yeh, H.-Y., Yeh, Y.-H., Wu, F.T., 1998. Two-dimensional crustal structures of Taiwan from gravity data. *Tectonics* 17, 104–111.
- Yu, H.-S., Chou, Y.-W., 2001. Characteristics and development of the flexural forebulge and basal unconformity of Western Taiwan Foreland Basin. *Tectonophysics* 333, 277–291.
- Yu, S.-B., Chen, H.-Y., Kuo, L.-C., 1997. Velocity field of GPS stations in the Taiwan area. *Tectonophysics* 274, 41–59.